PB-214 506

EXPERIMENTAL DETERMINATION OF THE COMPRESSIVE BEHAVIOR OF A LINEAR INDUCTION MOTOR REACTION RAIL

E. C. Haight, et al

Mitre Corporation
McLean, Virginia

1 November 1972

BIBLIOGRAPHIC DATA SHEET	1. Report No.	2.	3. Recipient's Accession No. PB-214 506
4. Title and Subtitle: EXPERIMENTAL DETERMINATION OF THE COMPRESSIVE BEHAVIOR OF A LINEAR INDUCTION MOTOR REACTION RAIL			5. Report Date: November 1, 1972 6.
7. Author(s): E. C. Haight, W. A. Hutchens(MITRE); J. G. Williams(NASA)			8. Performing Organization Rept. No. MTP-374
9. Performing Organization Name and Address: The MITRE Corporation Westgate Research Park McLean, Virginia 22101			10. Project/Task/Work Unit No. 1500/150F 11. Contract/Grant No. FR-7-35248
12. Sponsoring Organization Name and Address: U. S. Department of Transportation Federal Railroad Administration Advanced Systems Division, Office of Research			13. Type of Report & Period Covered Feb.-May 1972 MITRE Tech. Paper 14.

15. Supplementary Notes

COLOR ILLUSTRATIONS REPRODUCED IN BLACK AND WHITE

16. Abstracts

The reaction rail provides guidance for and reacts the thrust of the motor in the Department of Transportation's Linear Induction Motor Research Vehicle (LIMRV). The tests described in this paper provide data which lead to the understanding of the behavior of the rail in compression. Tests were performed to determine the buckling load and buckling mode shape, the effect of initial imperfections on static lateral stability, and the effect of compressive forces on rail lateral stiffness. Included is a recommendation for an improved field installation.

17. Key Words and Document Analysis. 17a. Descriptors

High Speed Ground Test Center
Ground Transportation
Linear Induction Motor Reaction Rail

17b. Identifiers/Open-Ended Terms

17c. COSATI Field/Group

18. Availability Statement	19. Security Class (This Report)	21. No. of Pages
Release Unlimited	UNCLASSIFIED	82
	20. Security Class (This Page) UNCLASSIFIED	22. Price $3.00

MTP-374

PB 214 506

Determination of

Experimental Determination of the Compressive Behavior of a Linear Induction Motor Reaction Rail

EDWARD C. HAIGHT

WALTER A. HUTCHENS

The MITRE Corporation

JERRY G. WILLIAMS

National Aeronautics and Space Administation

Langley Research Center

NOVEMBER 1, 1972

ABSTRACT

The reaction rail provides guidance for and reacts the thrust of the motor in the Department of Transportation's Linear Induction Motor Research Vehicle (LIMRV). The tests described in this paper provide data which lead to the understanding of the behavior of the rail in compression. Tests were performed to determine the buckling load and buckling mode shape, the effect of initial imperfections on static lateral stability, and the effect of compressive forces on rail lateral stiffness. Included is a recommendation for an improved field installation.

ACKNOWLEDGMENT

The authors gratefully acknowledge the contributions of Kenneth Williams, James Kiss, and Powell Mitchell of the Operations Support Division of the Langley Research Center for conducting the laboratory tests, James Summerfield of Langley's Research Facilities Engineering Division for designing the end fixtures and other special equipment, and Martha LeVan of The MITRE Corporation for reducing the data and plotting the results.

TABLE OF CONTENTS

LIST OF ILLUSTRATIONS

LIST OF ILLUSTRATIONS (Continued)

LIST OF TABLES

SECTION I
INTRODUCTION

The U.S. Department of Transportation, Federal Rail Administration, Office of Research, Development and Demonstrations, currently has a linear induction motor (LIM) driven vehicle operating at its High Speed Ground Test Center near Pueblo, Colorado. This vehicle, which runs on a conventional railroad track, has a maximum speed capability of about 250 mph. The motor thrusts against, and is guided by, a vertical reaction rail which is a tall, thin, plate-like structure fastened along the centerline of the crossties of the track. Figure 1 shows the vehicle, the track and the reaction rail.

The LIM reaction rail is a one-piece, 6061-T6 aluminum alloy extrusion, supplied in lengths of 80 to 100 feet, and fusion welded on site into a continuous strip. The rail was installed in the spring of 1971 by preheating it to 140°F and clamping it to the crossties. Since the expected rail temperature extremes for the Pueblo site are +140°F to -30°F, the rail as installed should never experience compressive loads. The maximum average tensile stress, which occurs at -30°F, is approximately 22,500 psi.

During the winter of 1971-1972, the temperature at the test site fell to approximately -20°F and caused eleven total separations of weld joints and severe cracking and yielding in numerous others. Part of the difficulty has been attributed to poor quality control exercised in welding the joints and techniques have been developed to improve the weld strength. Nevertheless, the maximum tensile stress is still closer to the tensile yield stress of the material than is desirable. A reduction in tensile stress could be achieved by reducing the installation temperature. However, if the tensile stress is lowered at the low temperature end of the range of thermal excursions, then compressive stress will occur at the high temperature end.

Subjection of the rail to axial compressive stresses makes it necessary to investigate its structural behavior under such loadings. The rail may show inadequate compressive structural characteristics for the Linear Induction Motor Research Vehicle (LIMRV) design either by buckling, by developing limited lateral deformations that cause problems with the dynamic behavior of the vehicle, or by having inadequate lateral stiffness to guide the linear induction motor. Since the rail is not installed perfectly straight, it is also desirable to determine the degree to which initial imperfections reduce the buckling stress from that for a perfectly straight rail. This investigation addressed only the static behavior of the rail; however, rail properties necessary for conducting a dynamic analysis were obtained.

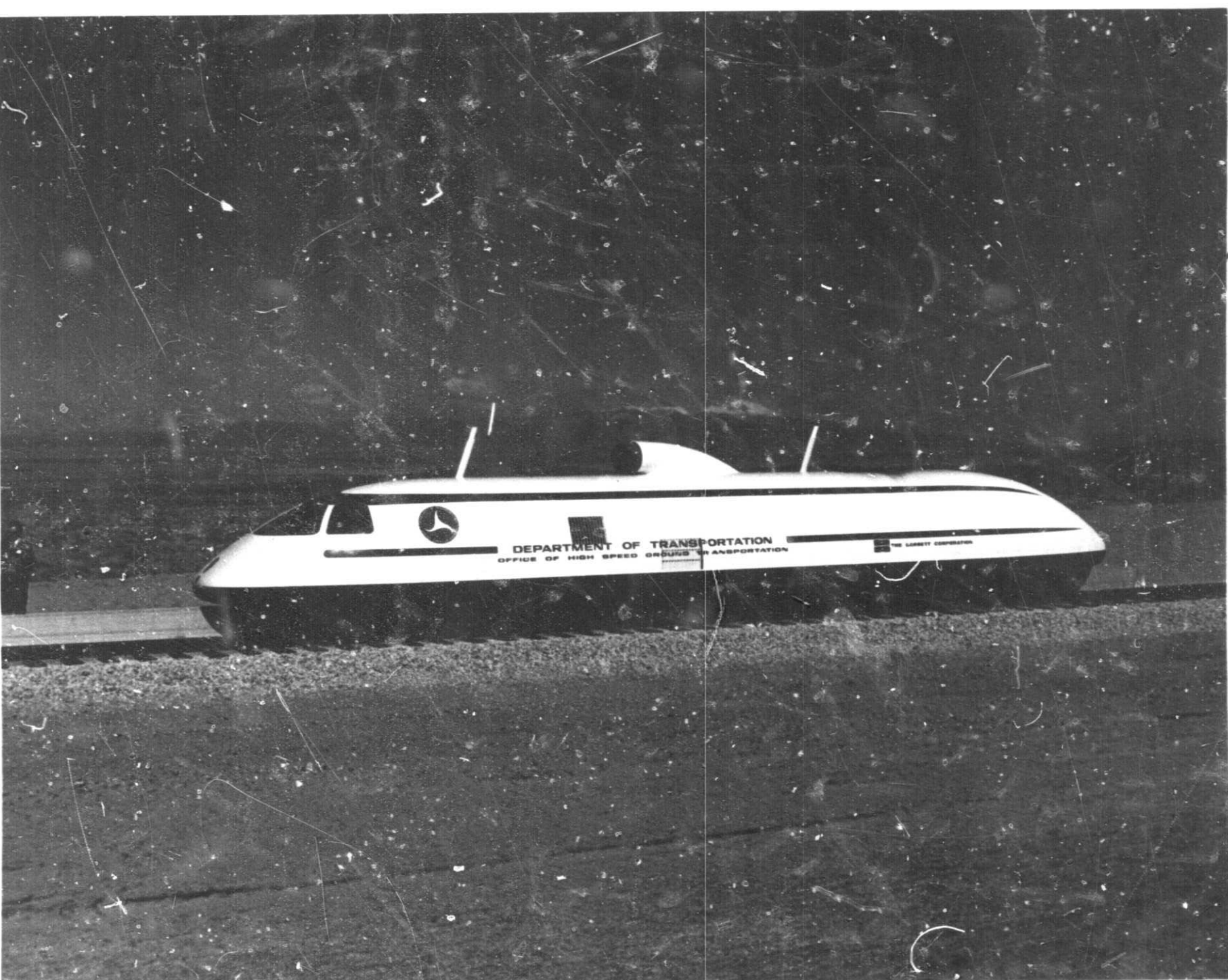
DEPARTMENT OF TRANSPORTATION

Specific items determined were:

1. the buckling load and mode shape
2. the lateral stiffness as a function of compressive stress
3. the effect of initial imperfections
4. whether or not buckling to large amplitudes is elastic

This information will serve two purposes. It

1. will be used as practical data regarding the behavior of the LIM rail under axial compression, and
2. serves to confirm and guide refinement of theoretical models of the rail for use in future design work for the Tracked Air Cushion Research Vehicle (TACRV) and other systems.

In order to collect the require ' data, a group of three experiments was carried out. All experiments were performed with the same basic test installation consisting of a 227" length of reaction rail mounted in a fashion as nearly representative of a good field installation as was practical.

The three tests were:

1. Buckling test of a "perfect"[1] rail. For this test, a "perfect" rail specimen was axially loaded until large lateral deformation appeared.
2. Buckling test of an initially imperfect rail. In this test, a full sine wave initial lateral imperfection with ±0.1 inch amplitude was imposed along the top edge of the specimen in its unstressed state. The rail was then loaded axially until large lateral deformations appeared.
3. Lateral stiffness test. This test was performed on a "perfect" rail. At various levels of axial compression, a lateral load was applied near the top edge at the rail midlength. The lateral load divided by the resulting displacement is defined as the lateral stiffness.

[1]The term "perfect" rail refers to a specimen which has been installed so that it is as nearly perfectly aligned on the laboratory test bed as is possible to make it. The alignment achieved was substantially better than the normal field installation.

The reaction rail is fastened to the ties by means of spring clips. Most analytical modeling of the rail system was based on the assumption that these clips perfectly restrained the rail base flange at the points where they contacted it. In order to verify this assumption, a series of tests of the clip and related parts was performed; these tests are described in detail in Appendix I.

Each of the three major experiments was performed more than once in order to have assurance of repeatability of the data. Two different rail specimens were tested; a third specimen was available as a backup but was not used.

All tests were performed in the Structures Laboratory at the Langley Research Center of the National Aeronautics and Space Administration. Planning and execution were accomplished jointly by MITRE and NASA personnel. The planning was accomplished during February and March of 1972 and testing was completed by the end of May.

SECTION II
GENERAL METHOD OF TESTING

AXIAL LOADS

All three experiments required variation of the state of axial stress of the test specimen. Two methods of accomplishing this variation were considered. First, a mechanical device can be used to compress the specimen by shortening it. Secondly, it is possible to heat the rail while restraining the ends. A variety of possible approaches exists for either method. The mechanical loading may be effected in some form of testing machine, or by jacking against one end of the rail with the other end restrained. The advantages of mechanical loading are simplicity (if the proper equipment is available), precise control of the axial displacement of the ends, and simple and direct control of the axial load. A disadvantage is that proper simulation of the end conditions is difficult to achieve in the laboratory. In addition, the use of a conventional universal testing machine makes a uniform displacement along the rail length difficult to achieve, especially in the presence of the restraining clamps along the rail base flange.

The second method would be to apply heat to a specimen which has its ends constrained against free expansion. The required thermal input might be obtained in various ways: by circulating a heated fluid through the voids in the rail section, by passing an electric current through the rail or through resistance wires in or on the specimen, or by radiant heating. A disadvantage of this loading method is that it is difficult to obtain a uniform temperature distribution in the specimen. A major advantage is that thermal loading is the method of compressing the rail in the field.

Thermal loading by means of quartz tube lamps placed in front of reflectors was chosen as the most practical method in view of the fact that the required equipment was readily available in the Structures Laboratory.

LATERAL LOADS

For the lateral stiffness test, a lateral load was imposed at the midlength of the test specimen using a hand operated hydraulic jack. The jack was mounted in a heavy steel frame which was bolted to the laboratory floor. Figure 2 shows a photograph of the test setup. For most of the tests the load was applied with a 2 1/2-inch diameter pad on the end of the jack ram. However, some tests used a 1/2-inch diameter steel ball mounted at the end of the jack extension rod in order to approximate more nearly a point loading condition. No significant differences were detected in the test results.

NASA
L-72-3158

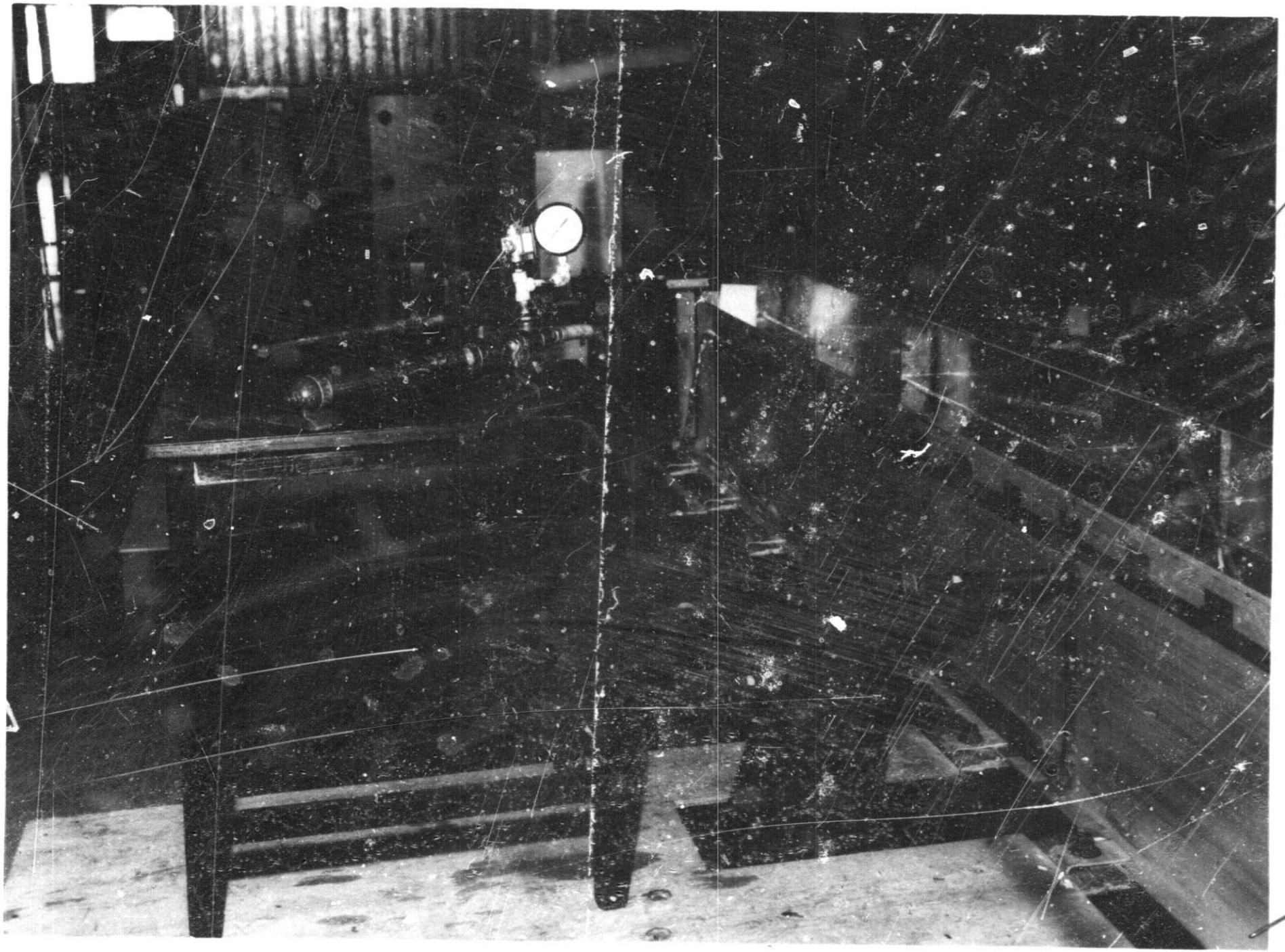

FIGURE 2
LATERAL LOADING APPARATUS

SECTION III
TEST SPECIMEN DESCRIPTION

The reaction rail used in the test program was selected from the stockpile of rail used for the test track installation at Pueblo. Three 227-inch-long specimens were cut from a segment initially 80 to 100 feet long which had passed the quality control inspection required for field use. Cross sectional dimensions and material properties for the rail are presented in Figure 3.

As delivered by the manufacturer to the field test site, the rail sections had noticeable irregularities. The manufacturing tolerances on these irregularities are given in Table I. Upon arrival in the laboratory, the test specimens were examined for initial straightness and freedom from defects and the specimens designated A and B were selected for the test series.

Measurements were made to determine the following properties for both specimens:

1. rail thickness variation in the longitudinal direction
2. rail thickness variation in the vertical direction
3. straightness of the flange in the lateral direction
4. straightness of the upper edge in the lateral direction
5. straightness of the base flange in the vertical direction

A large deep throat micrometer consisting of a C frame with a dial gage indicator was used to measure rail thickness at selected locations along the rail (see Figure 4). This instrument proved suitable for the relative thickness measurements desired in this application.

Straightness measurements utilized a surveyor's transit and level and a vernier height gage readable to 0.001 inch. Vertical measurements were made with the height gage upright and the level defining a horizontal plane, while for the lateral measurements the gage was horizontal and the transit defined a vertical plane. This system was found to yield data repeatable to about ±0.001 inch.

Rail surface-to-surface thickness was found to be substantially constant in the longitudinal direction, but varied noticeably in the vertical direction. A graph of the variation of this thickness in the vertical direction for specimen A is presented in Figure 5; this trend is typical of all three specimens. To determine the vertical variation of the

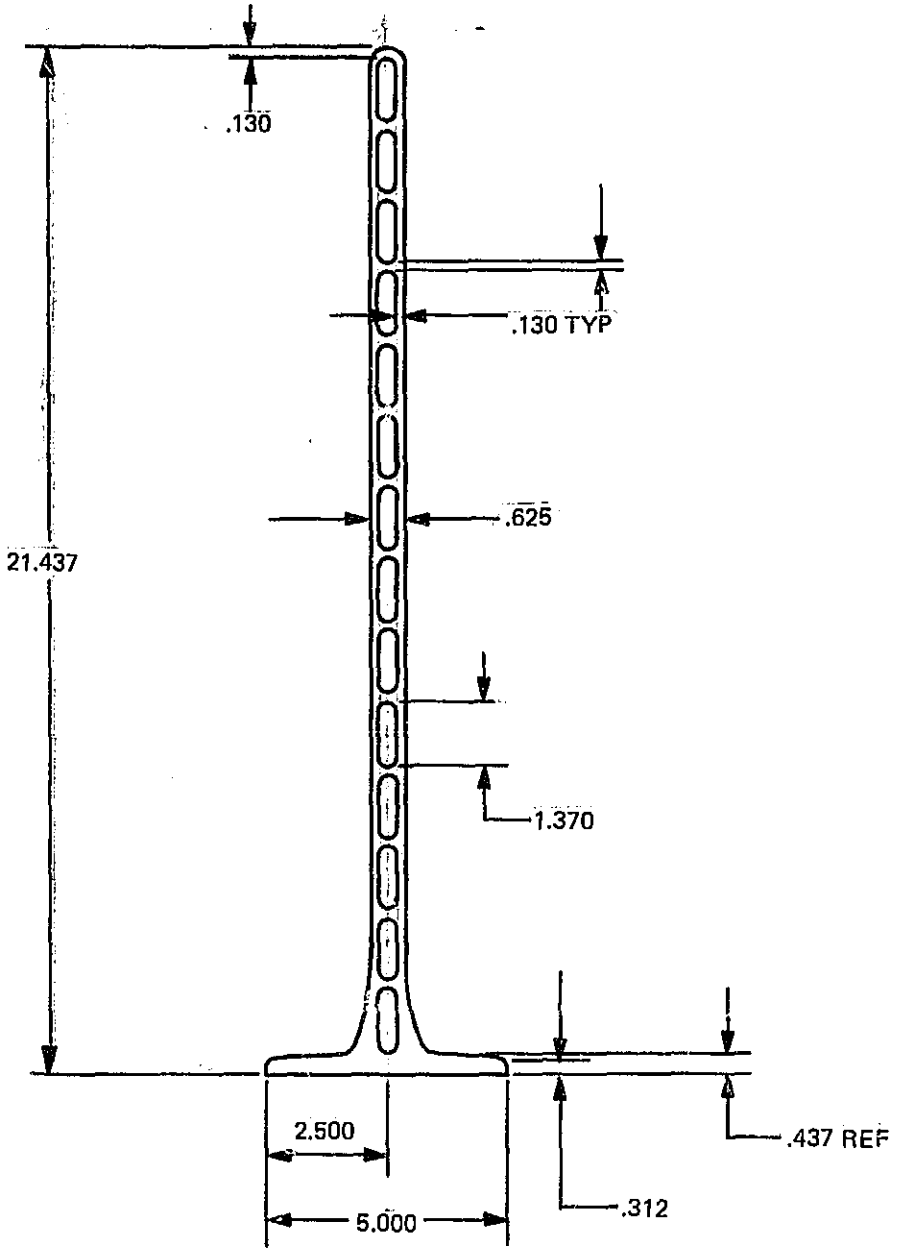

MODULUS OF ELASTICITY = 10^7 LB./IN.^{2}
POISSON'S RATIO = 0.3
CROSS SECTIONAL AREA = 8.67 IN.^{2}
COEFFICIENT OF LINEAR EXPANSION = 12.9×10^{-6} IN./IN./°F
WEIGHT PER FOOT = 10.41 LB.

FIGURE 3
DIMENSIONS AND PROPERTIES FOR THE REACTION RAIL

TABLE I

LIM REACTION RAIL FABRICATION TOLERANCES[1]

		Required Tolerance
(a)	Deviation of web thickness from nominal	±0.015 in. max at any point
(b)	Deviation of web from perpendicular to flange	±1.0 degree at any point
(c)	Deviation of web from straightness in longitudinal direction	±0.5 in. max in 50 ft. ±0.0125 in. max in 1 ft.
(d)	Deviation of web from flatness in vertical (transverse) direction	±0.08 in. max ±0.004 in. max in 1 in.
(e)	Longitudinal rate of change of web from flatness in vertical direction	±0.1 in. max per 50 ft. ± 0.01 in. max per 1 ft.
(f)	Deviation of flange width from nominal	±0.034 in. max in 50 ft.
(g)	Deviation of width of shoulders of tie plate from nominal	±0.05 in. max
(h)	Tie plate thickness under flange	±0.012 in. max
(i)	Twist of reaction rail section measured on bottom of flange	±3.0 deg max in 50 ft. ±0.25 deg max in 1 ft.
(j)	Straightness of top of rail in vertical (transverse) direction	±0.02 in. max in 1 ft.
(k)	Height of reaction rail	±0.124 in. max
(l)	Depth of surface defect	±0.003 in. max, may include roll marks

[1] Linear Induction Motor and Test Vehicle Design and Fabrication, AiResearch Manufacturing Company, Volume II, Book 2, Report 71-7094, p. B4-2.

NASA
L-72-2764

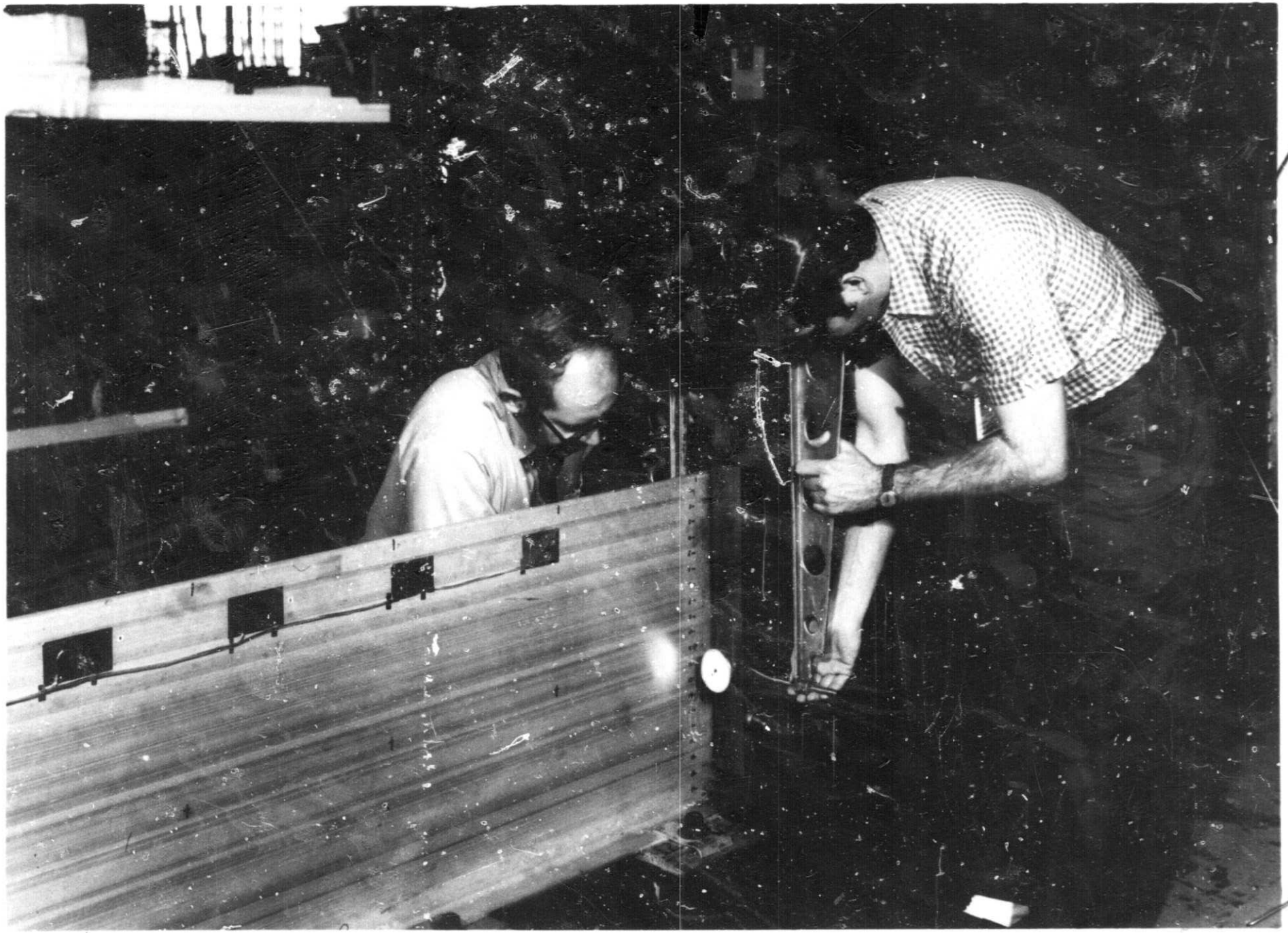

FIGURE 4
RAIL THICKNESS MEASUREMENT TECHNIQUE

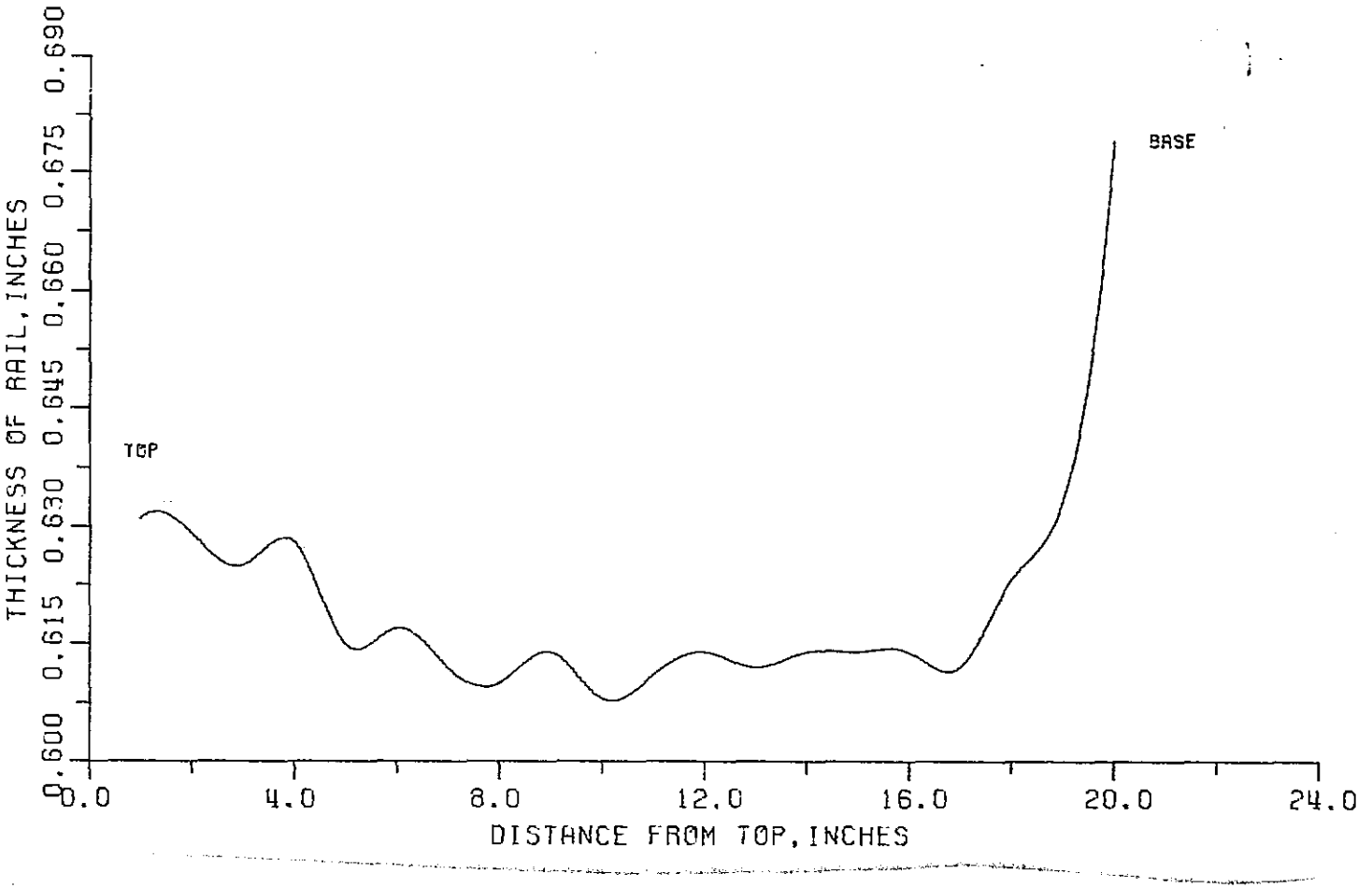

FIGURE 5
RAIL THICKNESS IN VERTICAL DIRECTION FOR SPECIMEN A

straightness of the base flange, the rails were held in the inverted position by supporting their flanges between two tables and the flange elevation was measured. Figure 6 shows results of this measurement for specimen B. The initial lateral straightness of the base flange and the initial lateral straightness of the upper edge of specimen A are shown graphically in Figure 7.

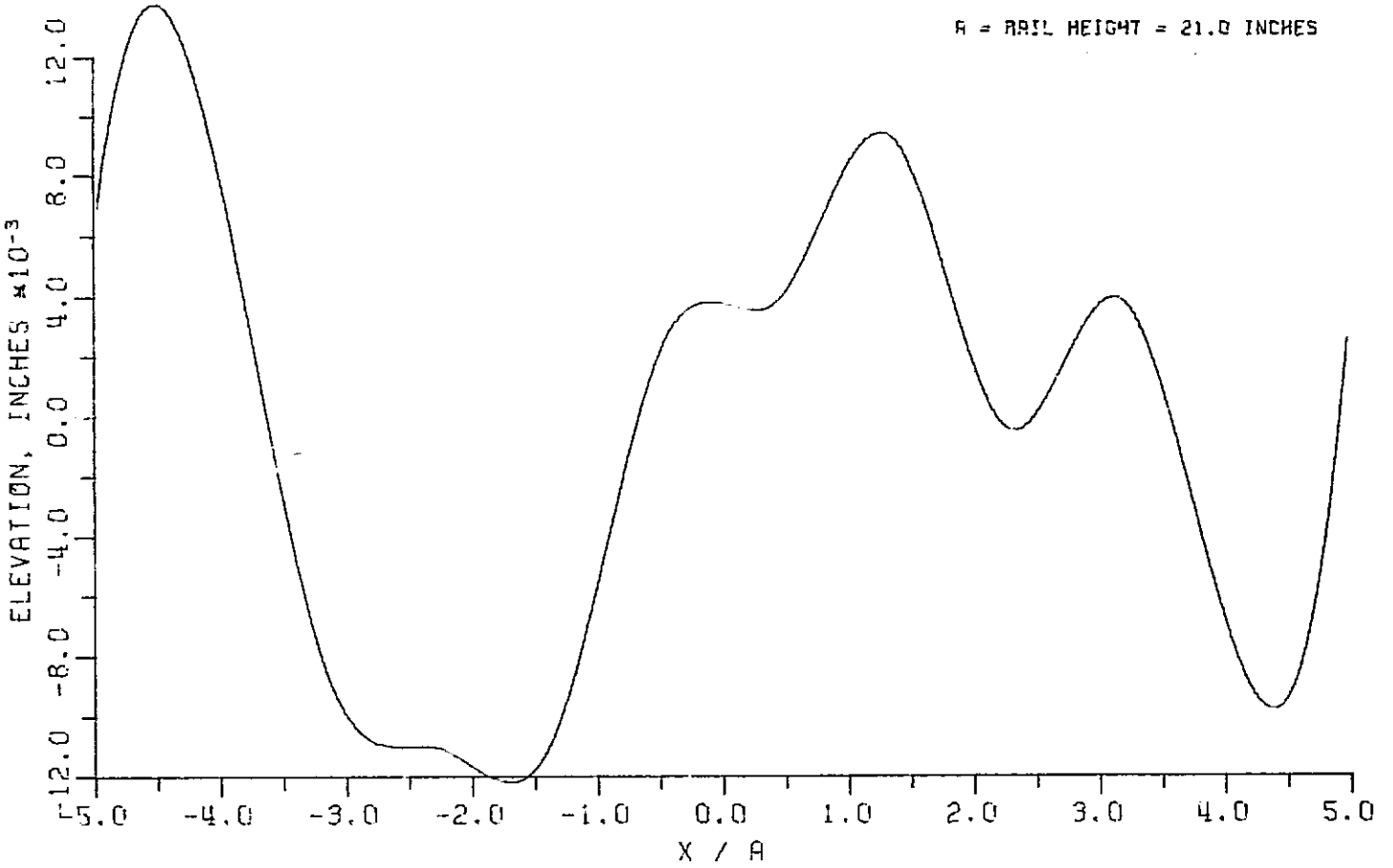

FIGURE 6
VERTICAL VARIATION OF STRAIGHTNESS OF THE
BASE FIGURE FOR SPECIMEN B

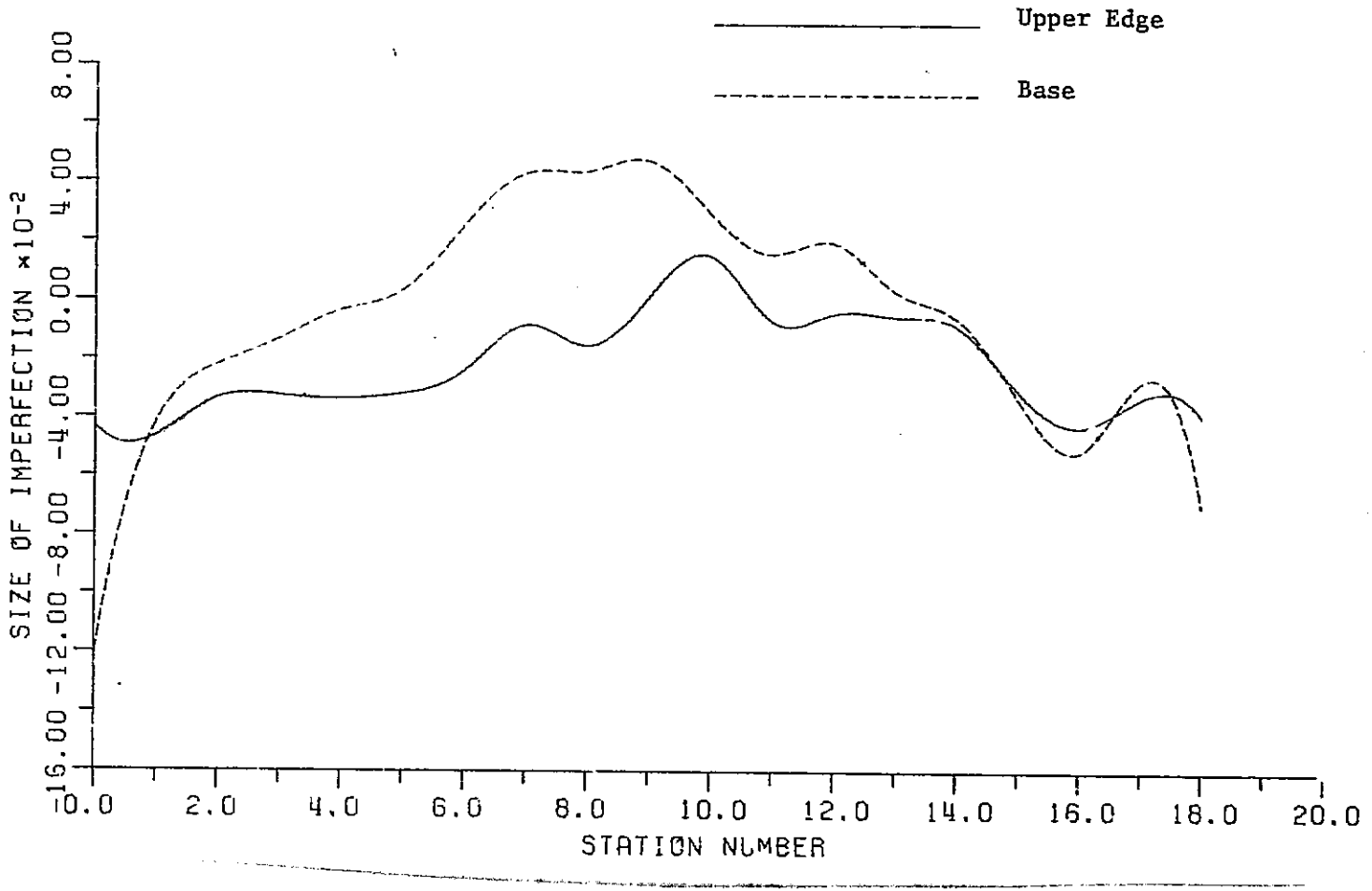

FIGURE 7
INITIAL LATERAL STRAIGHTNESS OF RAIL SPECIMEN A

SECTION IV

DESCRIPTION OF THE TEST INSTALLATION

REACTION RAIL SUPPORT STRUCTURE

In the field installation, the reaction rail is fastened to the centerline of wood crossties that are imbedded in conventional rock ballast. The reaction rail is mounted on aluminum tie plates and secured by steel clips. The running rails are also fastened to the crossties and have a standard gauge dimension (58-1/2 inches, inside-to-inside of the rail heads).

Because of the difficulty of precisely determining the support conditions resulting from the field installation it was desired to duplicate this installation insofar as practical in the laboratory. For the laboratory installation the crossties were fastened to a wooden subfloor constructed of two parallel 4 x 4 inch stringers located 60 inches apart. These were bolted to the floor using bolts through the stringers into tapped holes in the steel wide flange beams which are part of the very deep reinforced concrete floor system. The crossties were spaced 19 inches on center as they are in the field. Twelve crossties were used in the test installation.

The mounting system for the reaction rail is shown in Figure 8. At each crosstie it consists of one tie plate, two spring steel clips, two coach screws, and the necessary number of vertical and lateral shims. The tie plates are aluminum extrusions formed to accept the base of the rail and have two drilled holes for passage of the coach screws. Shims of various thicknesses are placed under the tie plate for vertical alignment and between the shoulder of the plate and the edge of the flange of the reaction rail for lateral alignment. Figure 9 shows the detail of each piece of mounting hardware.

END CONDITIONS AND FIXTURES

The experiments were designed to obtain data regarding the behavior of the rail for a long, continuous field installation. Since the rail was expected to be at roughly uniform temperature throughout its length in the field, no longitudinal motion of any point on the rail would be expected during axial loading caused by thermal cycling. These conditions indicate that the laboratory setup should not allow longitudinal movement of the rail end but do not specify the degree of restraint against rotation about a vertical axis. A clamped end condition was selected as it seemed simplest to implement.

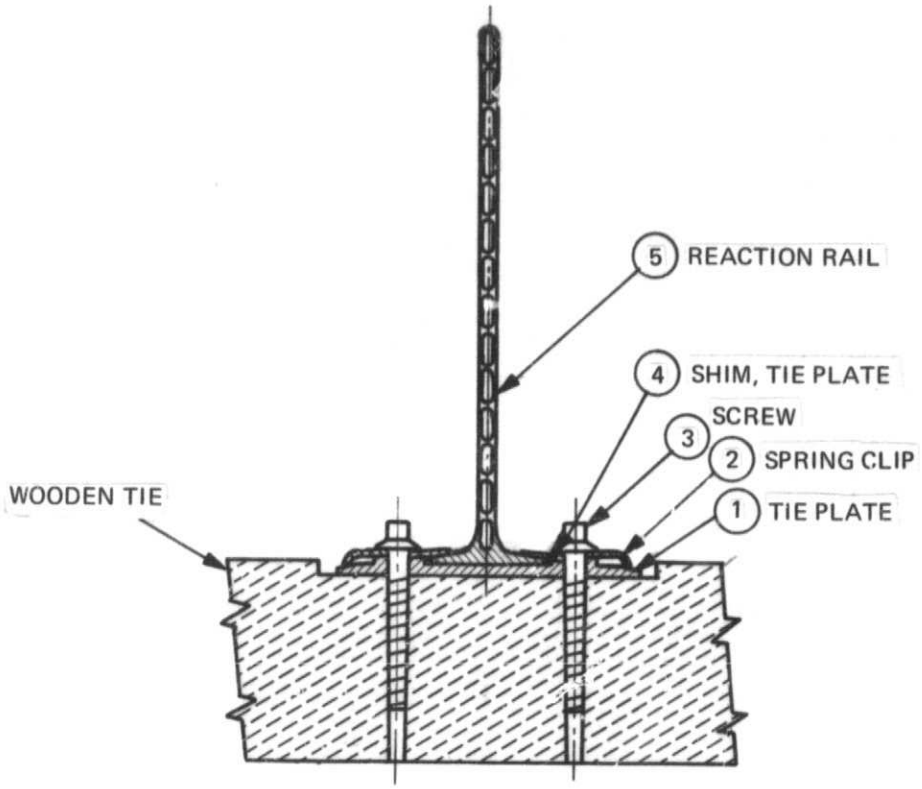

FIGURE 8
REACTION RAIL ATTACHMENT SYSTEM

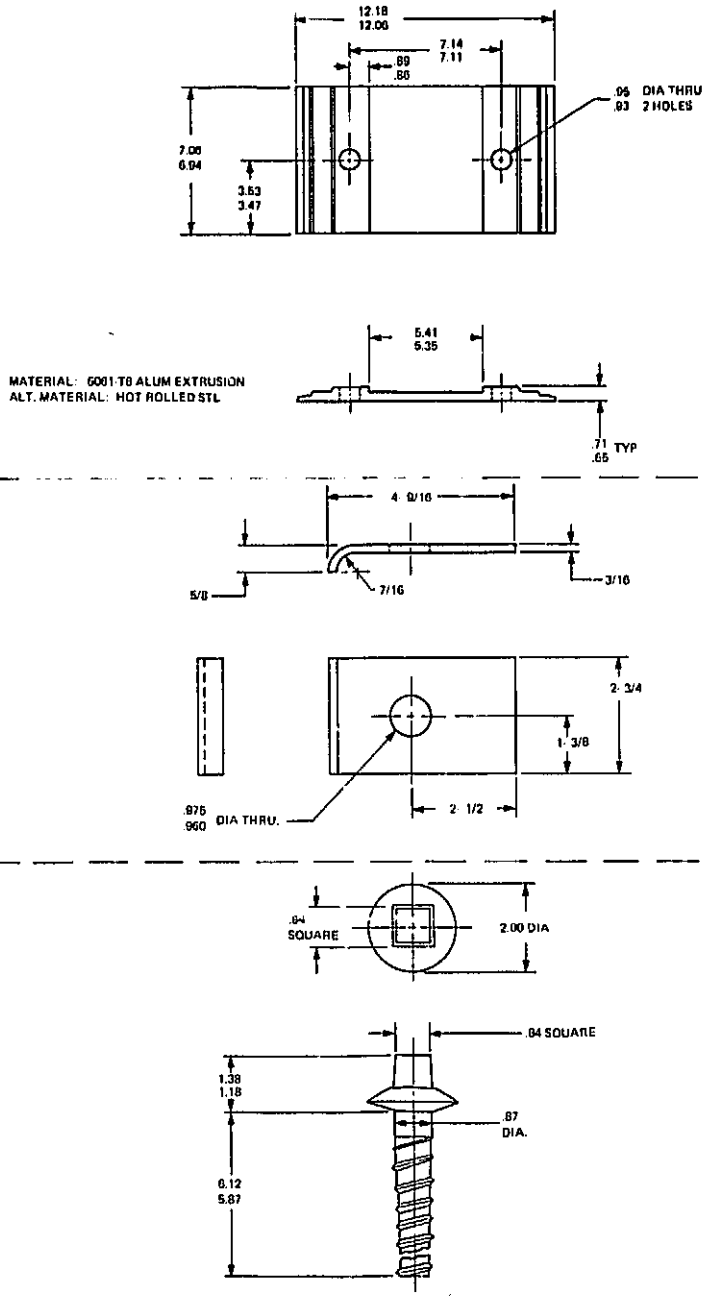

FIGURE 9
ATTACHMENT HARDWARE FOR REACTION RAIL

Figure 10 shows one of the two end fixtures. Each fixture consists of two parts as shown in the figure: an end billet into which the rail ends fit, and an end frame that cradles the end billet.

The end fixtures must provide restraint against longitudinal expansion; however, they must be so designed as to minimize the chance for local failure of the rail at or near its ends. This means that local non-uniformity of loading must be minimized. In order to distribute uniformly the longitudinal load over the rail cross-section, a flat bearing surface was machined into the billet for acceptance of the specimen end. Adjustment capability in the plane of the specimen was provided by movement of the billet relative to the end frame. The outer edge of the billet was chamfered to prevent a line stress concentration on the rail end. Leveling pads were used to align the billet in the frame.

The end frame was a welded structure which transfered loads from the rail/end billet assembly into the floor. High strength bolts were used to anchor the frame to a steel beam in the floor. Longitudinal restraint was improved for tests on Specimen B by attaching a square 14 inch by one and one-half inch thick plate to the laboratory floor and filling the one-fourth inch gap between the plate and the end frame with a glass-filled epoxy mixture.

HEATER SYSTEM

Two heater panels composed of seven rows of tubular quartz lamps backed by aluminum reflectors were constructed to heat the rail section being tested. The lamps were oriented parallel to the rail base and were spaced 3-1/2 inches apart. Each panel was 212 inches long and was positioned parallel to and approximately seven inches from each vertical surface of the rail.

The voltage applied to each panel was continuously variable up to 450 volts. At full rated power both panels would have had an output of 280 kilowatts; however, with the power supply used only 95 kilowatts was available.

Preliminary testing showed that the heating system caused a nonuniform temperature distribution in the rail with the top considerably hotter than the flange. This condition was judged undesirable because it caused non-uniform stress distribution. The non-uniform temperature distribution was partially attributed to an inrush of cool air under the heater panels striking the flange area of the rail. To reduce this effect and to protect

NASA
L-72-2631

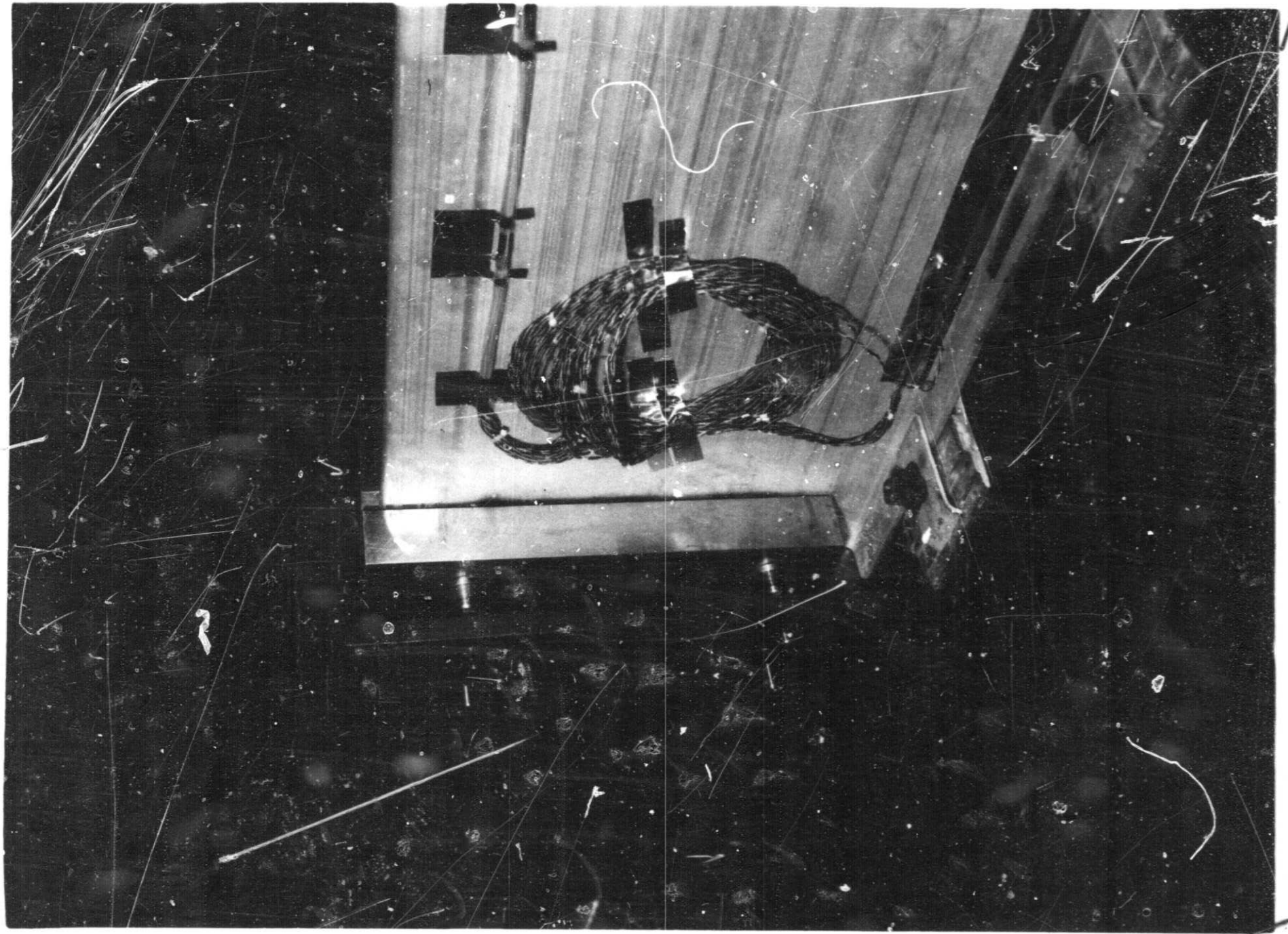

FIGURE 10
END FIXTURE

the combustible ties from excessive heat, the exposed parts of the ties between the rail and heater panel and the spaces below the panels were covered with sheet asbestos. To further improve uniformity of rail temperature, the second and fourth rows of lamps from the top of the initial seven rows on each heater panel were removed thus reducing the heat flux to the upper half of the rail.

By using these measures it was found that the rail temperature quickly evened out to within a few degrees when the heater power input was briefly reduced. As a result, a stepped voltage time history applied for the heater panels was used for the buckling tests to allow measurements to be made during periods of near uniform temperature.

SECTION V
TEST INSTRUMENTATION

Strain, temperature, displacement and lateral load measurements were taken during the tests. Most of the data were automatically recorded on magnetic tape for later reduction. Other data were recorded manually or observed on an electronic scope. Layout drawings locating the positions at which measurements were taken and detailing the instrument numbering scheme for the two test specimens are presented in Appendix II.

STRAIN GAGES

Temperature compensated wire resistance strain gages were attached with epoxy resin to specimens A and B at the locations shown in Figure AII-1. Strain gages were connected in a conventional three lead circuit in order to cancel the effect of temperature induced changes in the lead resistance. The strain gages were covered with aluminum foil tape for mechanical protection and to minimize excessive heating of the gages by the lamps. Strain data was collected by the automatic data recording system for later reduction.

A calibration test was conducted to measure the variation in gage factor as a function of temperature. Data was corrected for this apparent thermal strain and converted to stress using the biaxial stress relationships. In this calculation the principal directions were taken to be horizontal and vertical.

THERMOCOUPLES

Iron-constantan thermocouples were used to measure the rail temperature at the points shown in Figure AII-2. In order to assure a good thermal connection to the rail, the beads of these thermocouples were imbedded in punch marks in the rail surface. The response of a set of thermocouples located near the center of the specimen in a vertical line on both sides of the rail was recorded on a strip chart during each test. The uniformity of these readings from side to side and top to bottom was used as an indicator for making adjustments in the lamp voltage applied to the heater panels on each side of the rail and for controlling the heating rate. In addition, thermocouple data were recorded by the automatic data recorder system.

DISPLACEMENT MEASUREMENTS

Most of the displacement measurements in the test series were made using linear voltage displacement transformers (LVDT) as shown in Figure 11. Since the response of

NASA
L-72-2870

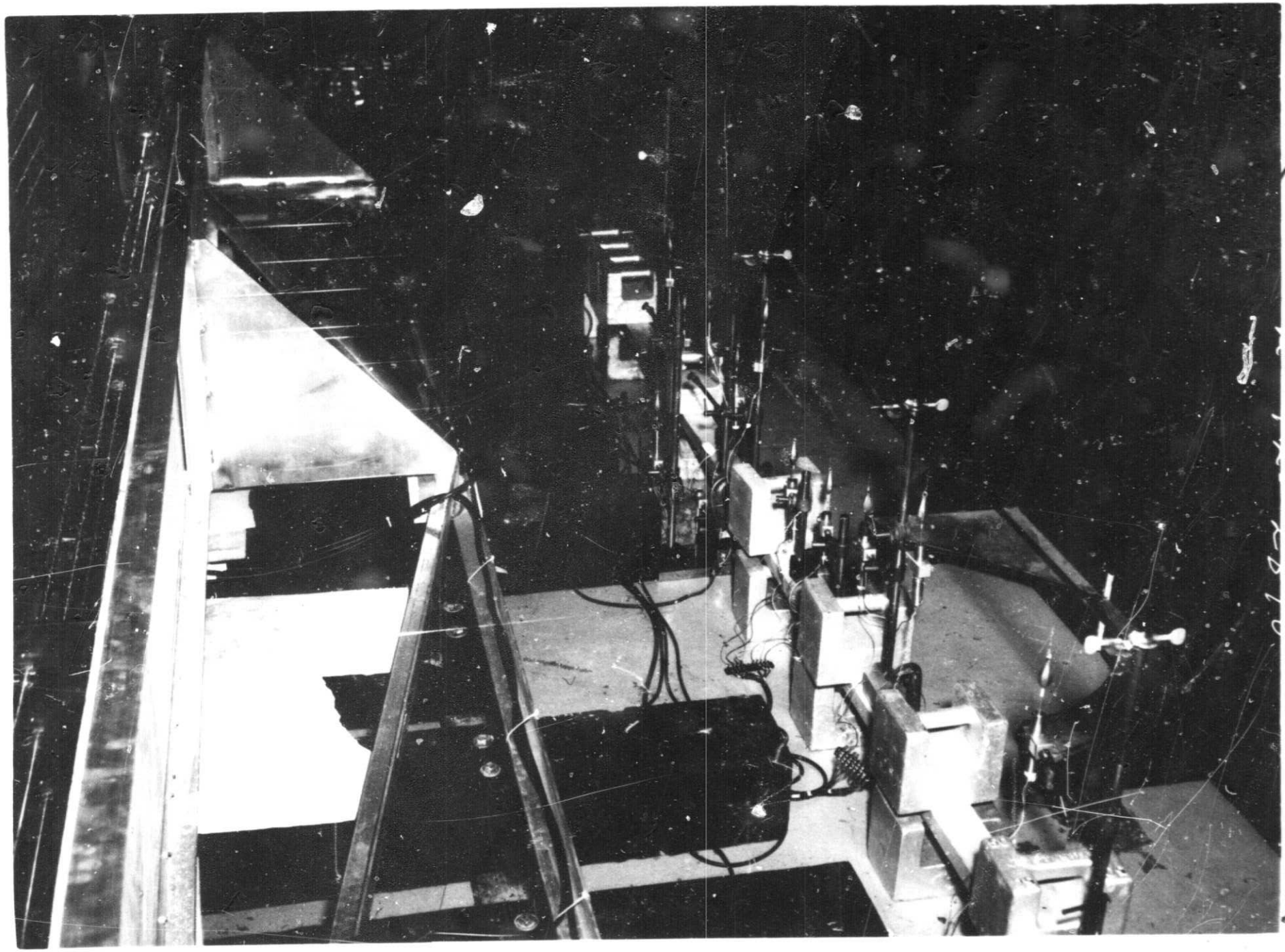

FIGURE 11
LVDT SETUP

these instruments is affected by heat and by proximity to strong magnetic fields it was necessary to locate them away from the heater panels. This was accomplished by bonding one end of a fibreglass string to the point on the rail at which displacement was to be measured, and leading it away from the rail in the direction of expected motion over one or more guide rods to a vertically mounted LVDT having a lead weight on the lower end. The LVDT arrangement is shown in Figure AII-3. Outputs of these instruments were monitored locally on a storage oscilloscope. In addition, all LVDT's were connected to the automatic data acquisition system.

Measurement of the axial displacement of the end fixtures was accomplished with the aid of dial indicators which were graduated in 0.001-inch increments. These measurements allowed assessment of the degree of restraint provided by the specimen end fixtures.

SECTION IV
TEST DESCRIPTIONS

This section presents a detailed description of the three separate experiments.

Prior to each test the rail was surveyed and, when necessary, shims were used to obtain the necessary conditions of straightness. A graphical representation of a typical vertical alignment of the tie plates is presented in Figure 12. For the "perfect" rail experiment the upper edge and base were laterally aligned within ±0.015 inch and ±0.005 inch, respectively, of a straight line drawn through the end points of the rail (see Figures 13 and 14 for typical lateral alignment results). This alignment is substantially better than that normally achieved in the field installation.

BUCKLING OF A "PERFECT" RAIL

The purposes of the buckling test on the "perfect" rail specimen were:

1. to determine an experimental upper bound for the buckling load,
2. to determine the characteristic buckling wave shape, and
3. to determine whether large amplitude buckling is elastic.

The reason for the third purpose lies in the answer to the question, "Is buckling acceptable in the operational test system in the field?" Buckling might well be acceptable provided the vehicle is not being operated at the time and all traces of the lateral deformation disappear when the temperature is reduced.

This test was conducted on a rail specimen aligned as perfectly as possible as described in Appendix III–Test Specimen Installation Procedure. All instrumentation was zeroed at room temperature and the voltage to the heater panels was gradually increased. A small number of the LVDT's and thermocouples were monitored during the test and the remainder of the data were recorded automatically for later reduction. There was no manual interaction by the test operators with the experiment except to adjust the lamp voltage in order to control the temperature.

This experiment was carried out a total of four times as summarized in Table II.

BUCKLING OF AN INITIALLY IMPERFECT RAIL

The reaction rail as installed in the field has a variety of lateral imperfections. Some of these were created during the installation process and others have grown through use of the rail for test purposes. The purpose of the buckling tests on the initially imperfect rail was to assess the effect of typical irregularities on the rail compressive behavior.

FIGURE 12
ELEVATION OF TIE PLATES AFTER SHIMMING

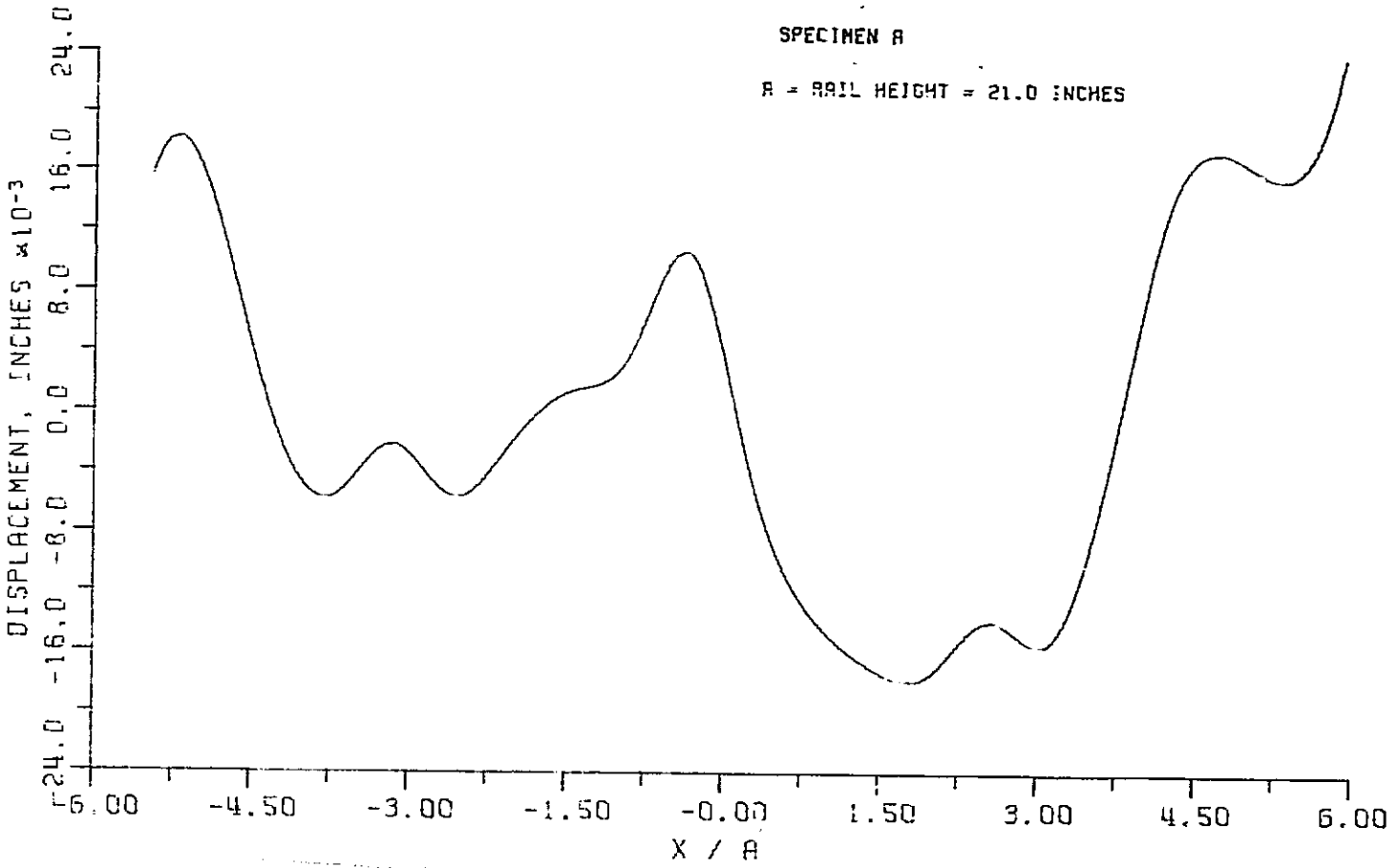

FIGURE 13
LATERAL ALIGNMENT OF RAIL UPPER EDGE AFTER SHIMMING

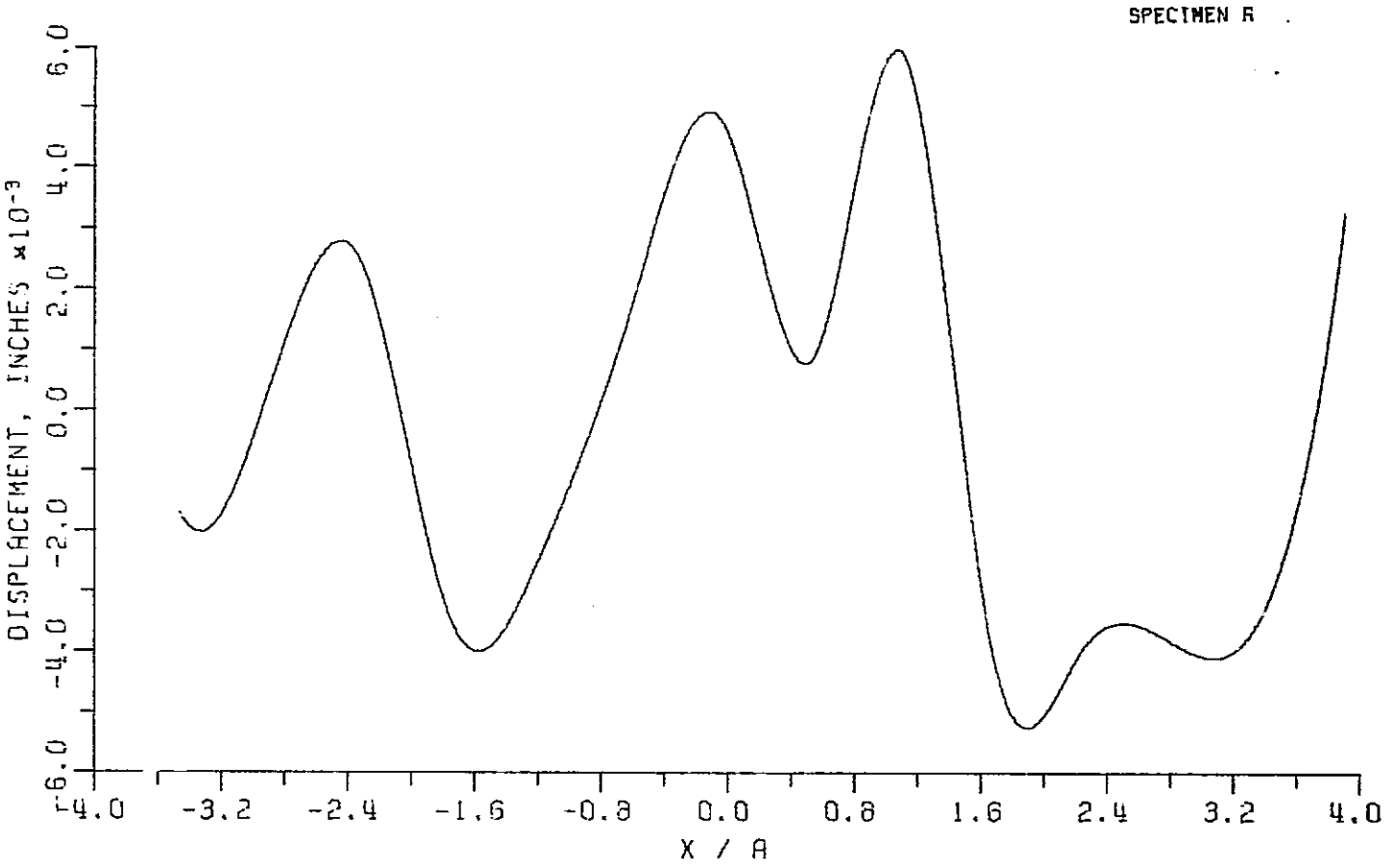

FIGURE 14
LATERAL ALIGNMENT OF RAIL FLANGE AFTER SHIMMING

TABLE II

RAIL TESTS

Experiment	Test/Run Numbers	Specimen	Date	Remarks
"Perfect" Rail Buckling	425/2	A	23 April	Preliminary test. Terminated prior to buckling.
"Perfect" Rail Buckling	425/3 & 4	A	24 April	Single test, successful. Maximum amplitude about 0.2 inches.
"Perfect" Rail Buckling	427/1	B	25 May	Successful. Maximum amplitude 0.10 in.
"Perfect" Rail Buckling	427/2	B	25 May	Successful. Maximum amplitude 0.75 in.
Initial Imperfection	425/7	A	4 May	Successful. Maximum amplitude 0.5 in.
Lateral Stiffness	425/5	A	26 April	Poor data. Pressure transducer not used.
Lateral Stiffness	425/6	A	3 May	Successful. Pressure transducer used.
Lateral Stiffness	427/4	B	30 May	Successful. Included linearity check at room temperature.

The only data currently available on the size and shape of these irregularities is a crude set of measurements taken on a non-prestressed 90-foot segment at Pueblo. These data show that a predominant shape has a half-wavelength of ten feet with an amplitude of about 0.1 inch. This shape, a full sinusoid of 0.1 inch amplitude and having a node at the center and each end, was used for this part of the test program. Analytical work will be used to extend the study of the effects of initial irregularities to other imperfection shapes.

The conduct of this test was essentially the same as for the buckling test on the "perfect" rail except that shims were placed under the rail to tilt its upper edge into the sinusoidal shape. After zeroing the instruments at room temperature, the rail was heated until large amplitudes appeared. Only one of these experiments was performed as shown in Table II. The test was fully successful with a half-wave amplitude of 0.6 inches being developed.

LATERAL STIFFNESS TEST

The purpose of the lateral stiffness test was to determine the relationship between the lateral stiffness of the reaction rail and the axially applied compressive force. Lateral stiffness for the reaction rail can be defined generally as

$$k = \frac{\int_A q(x,y)dA}{\frac{1}{A}\int_A w(x,y)dA}$$

where A = area of rail surface covered by the lateral load

$q(x,y)$ = lateral force per unit area on the rail surface

$w(x,y)$ = lateral deflection function for the rail.

The above formula shows that the rail lateral stiffness is a function of loading geometry as well as the magnitude of the load.

The loading used in this test program was a lateral point load. Consequently, the above formula reduces to

$$k = \frac{F}{\delta}$$

where F = magnitude of the point load

δ = lateral deflection of the rail under the loading point.

The reason for using a point load rather than the actual field lateral loading configuration for the linear induction motor against the rail was one of simplicity. Complex load distributions are difficult to produce accurately. The immediate use of the experimental stiffness data was to confirm an analytical model of the rail. This could be done as effectively for a point load as for a more complex pattern. The analytical work could then be used to extend the results to more complicated cases.

For all the lateral stiffness tests, the point load was applied at the midlength of the specimen six inches below the upper edge. This point is approximately half-way between the upper and lower motor guidance wheels at one end of the LIM.

The test had two parts. The first part was a "calibration check" which consisted of two applications of load from 0 to about 1675 lb. at room temperature. The first loading was to take any free motion out of the specimen clamping system and the second was to check the linearity of the load-deflection behavior of the rail.

The second part of the test was to determine the relationship between lateral stiffness and axial load. To perform this test, the rail was placed in compression by heating it. It was found that better temperature uniformity could be achieved during cooling the rail than during heating it. Accordingly, the test was conducted by heating the rail to the highest temperature for which data was to be taken and then taking data at 5°F intervals during cooling. The cooling rate was controlled by reducing the lamp voltage in staircase units. With this procedure the maximum difference between temperatures at the base flange and the rail top was about 16°F and the maximum difference between the center and the rail end was about 65°F. To obtain a reading, a lateral load sufficient to cause on the order of three-eighths inch lateral displacement was applied and then released. The test was performed three times as shown in Table II. The first experiment used a simple gage on the hydraulic jack to measure pressure. The gage was found to be insufficiently accurate and the pressure transducer was installed on the jack for later tests.[1] The displacement of the rail surface directly opposite the jack point was measured by an LVDT. This data was sampled and recorded automatically as previously described. Figure 15 shows the lateral stiffness test in progress.

---

[1] A load cell would have given more accurate results; however, a suitable instrument was not immediately available.

NASA
L-72-3071

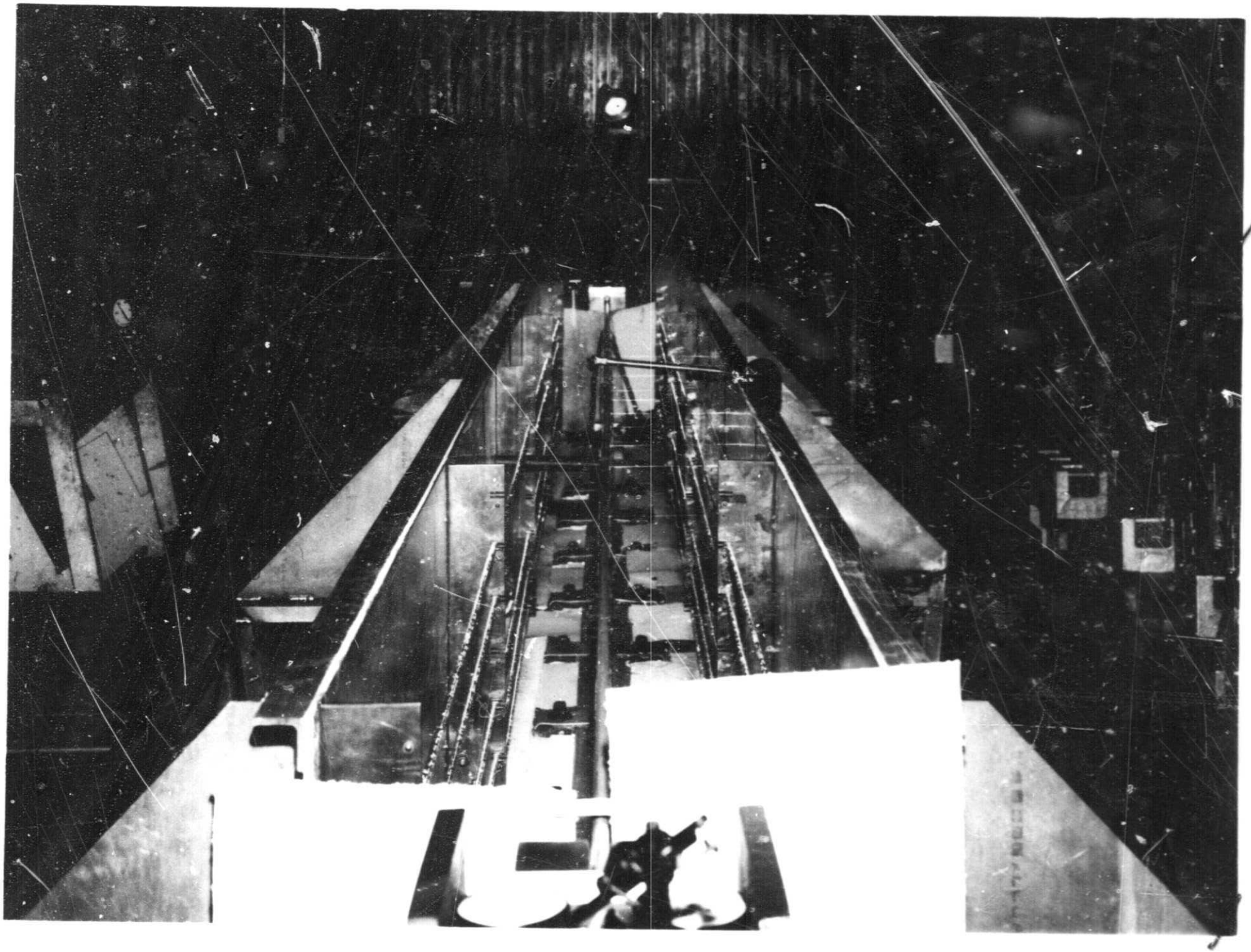

FIGURE 15
LATERAL STIFFNESS TEST IN PROGRESS

The principal difficulty with this test was one of stiction in the hydraulic jack. This was discovered by plotting the load-deflection data taken at the constant room temperature. This graph, although linear, had an intercept on the positive force axis. In other words, the data implied that a positive amount of lateral force caused no lateral deflection. To correct for this error, the force axis intercept was subtracted from all force readings for purposes of computing lateral stiffness.

SECTION VII
RESULTS

Before beginning the discussions of the specific test results, several general considerations which affected all the tests will be mentioned.

The end fixtures for this test were designed to be very stiff and each was bolted to a steel beam in the laboratory floor by twelve one inch diameter high strength steel bolts. Had perfect restraint and uniform rail temperature been realized the axial stress in the rail specimen would have been

$$\sigma_x = E\alpha\Delta T$$

where E is the modulus of elasticity

α is the coefficient of thermal expansion

and ΔT is the temperature differential referred to the stress-free temperature.

However, when heat was applied to the clamped rail specimen the end fixtures were found to move substantially. Evidently this behavior was due to the presence of some clearance in the bolt holes. Figure 16 shows the stress calculated from $E\alpha\Delta T$ and the stresses obtained experimentally for both specimens. As previously described, a bearing plate intended to give added restraint was added for specimen B. This installation produced about a 10% reduction in ΔT needed for a given stress level, as can be seen from Figure 16.

Such movement would definitely be unacceptable if one were to attempt to calculate buckling loads from rail temperature measurements alone. With strain gages present, however, the actual buckling stress can be calculated directly from the strain measurements. Movement of the end fixtures means that higher rail temperatures must be reached to produce the same axial stress level that complete end restraint gives. However, this added temperature increase was not sufficient to cause a significant change of material properties. For example, an increase in rail temperature from 150°F to 250°F reduces the modulus of elasticity for 6061 aluminum by only about 2%.[1]

Because the stress in the laboratory at temperature T_1 with end fixture slippage is less than the stress in the field at the same T_1 with complete restraint, it is useful to

---

[1] Metallic Materials and Elements for Aerospace Vehicle Structures, MIL-HDBK-5A, February 8, 1966, p. 328.

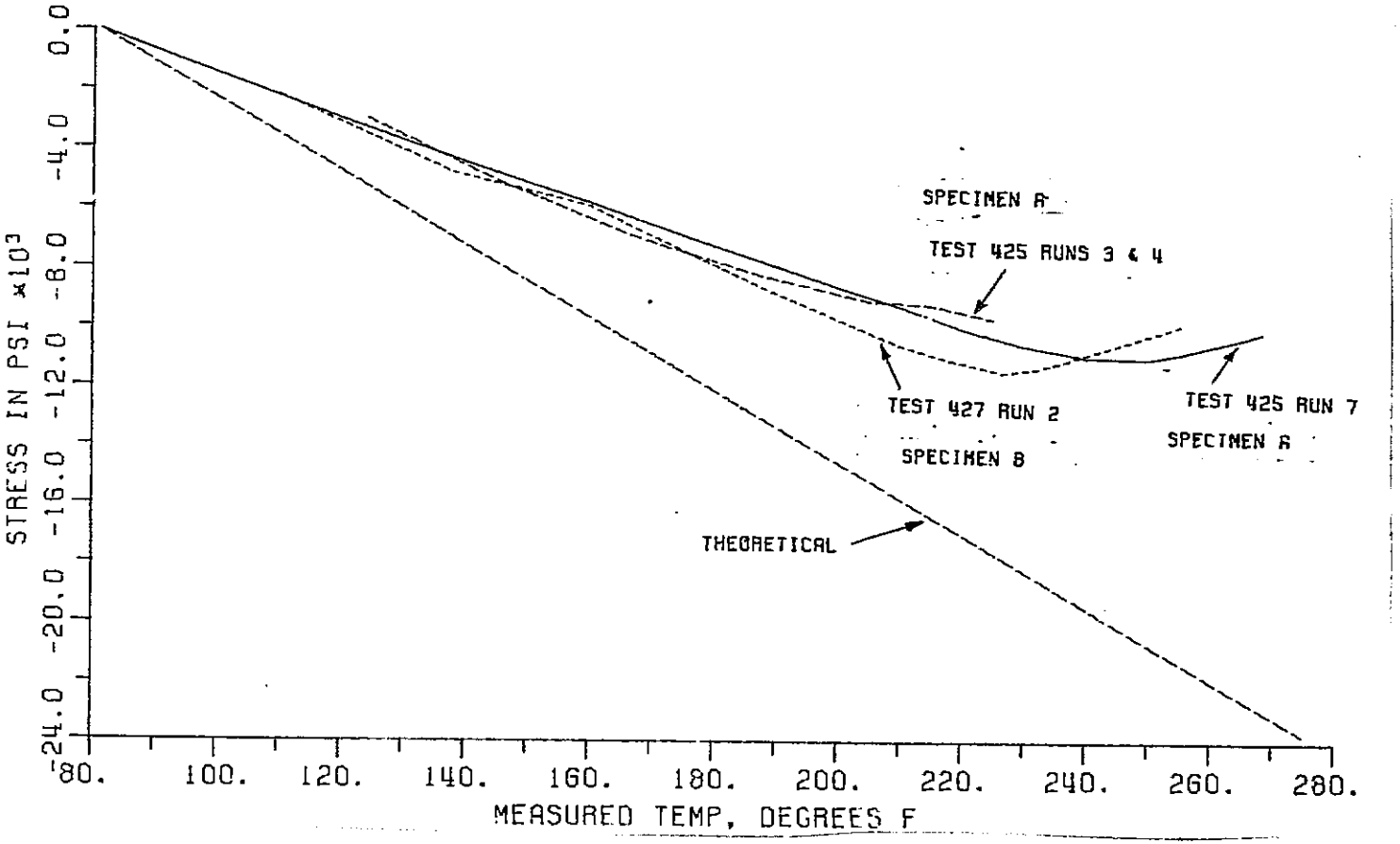

FIGURE 16
AXIAL STRESS VERSUS MEASURED TEMPERATURE

introduce the term "equivalent temperature rise". The equivalent temperature rise is the increase in rail temperature over the stress free installation temperature that produces a given axial stress level for a perfectly restrained rail. It is calculated from $\Delta T = \frac{\sigma}{E\alpha}$ where ΔT is the equivalent temperature rise and σ is the experimentally determined axial stress level. For example, Figure 16 shows that when specimen A was about 100°F above installation temperature, the axial stress was 7500 psi compression. Hence, the equivalent temperature rise T is 58°F.

Although a perfectly uniform temperature distribution over the entire plate is desired, this was not achieved for any of the tests. A profile of the temperature distribution in the rail which is typical for all tests in the series is presented in Figures 17 and 18 for the vertical and horizontal directions, respectively. The distribution at the rail center in the vertical direction shows the base flange temperature to lag the maximum temperature of the vertical portion by approximately 30°F in the worst case. The distribution along the rail length shows the temperature at the end to lag the temperature at the center by approximately 80°F at the maximum test temperature. Temperatures were lower at the rail ends due to the large metal end fixtures which acted as heat sinks and because the radiant energy flux was lower in the region of the ends since the heater panel terminated approximately six inches short of each end.

BUCKLING TEST RESULTS

As described previously, the buckling test consisted of heating a "perfect" rail specimen until large lateral deformation occurred. The buckling load of the test specimen can be determined by a number of techniques. The ones shown here are:

1. Stress versus maximum lateral displacement. The buckling load is defined by drawing a vertical tangent to the curve. The stress corresponding to the location of this vertical tangent is then taken as the buckling stress.
2. Southwell plot. The Southwell plot is a graph of lateral deflection divided by axial stress versus lateral deflection. The inverse slope of the graph is the buckling stress and the intercept on the abscissa is the magnitude of the initial imperfection.
3. Strain reversal. A graph of axial strain taken on opposite sides of the rail at its midlength near the top edge versus average axial stress at that point can also be

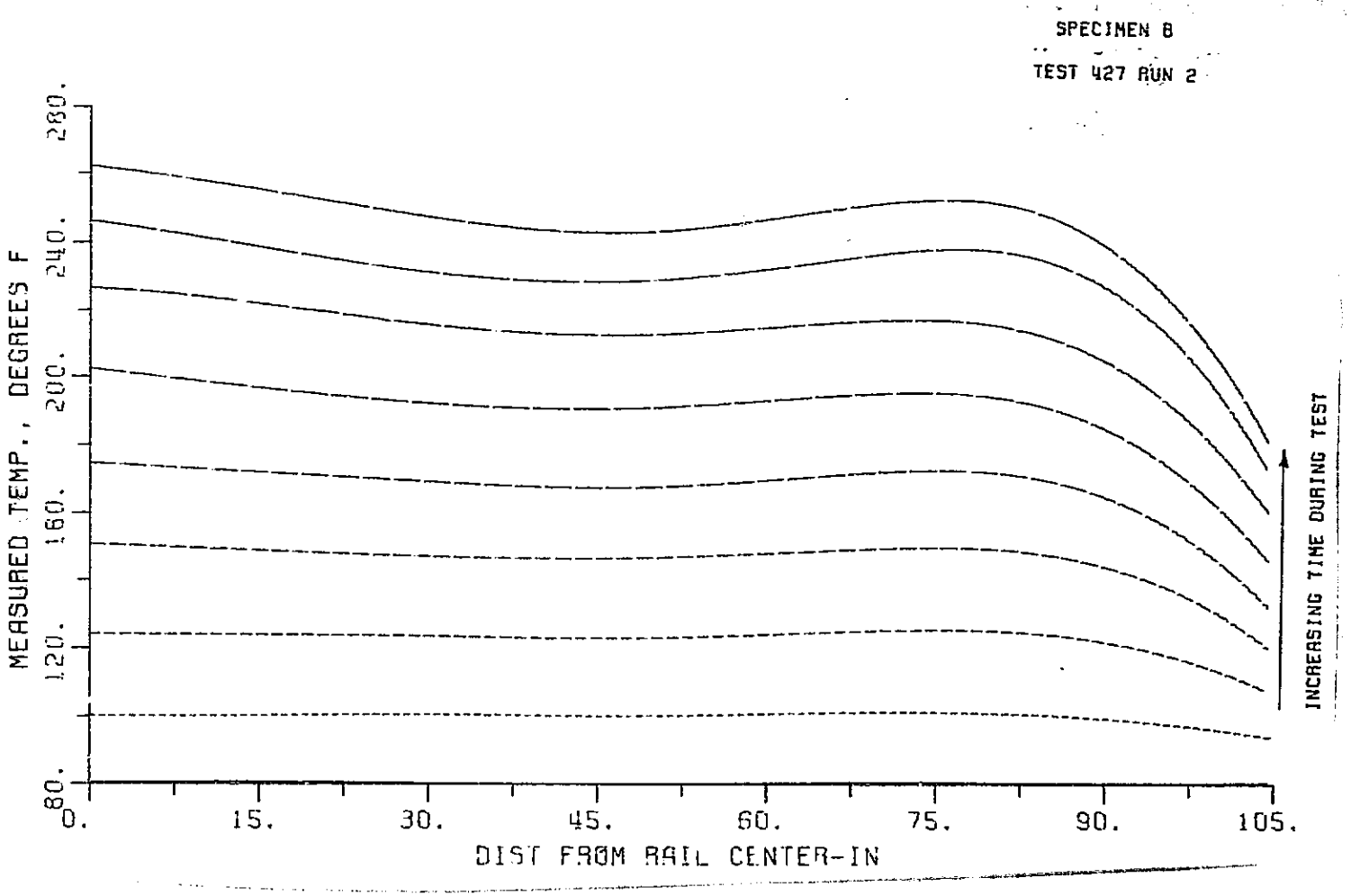

FIGURE 17
SELECTED TEMPERATURE PROFILES ALONG RAIL LENGTH FOR HALF OF RAIL

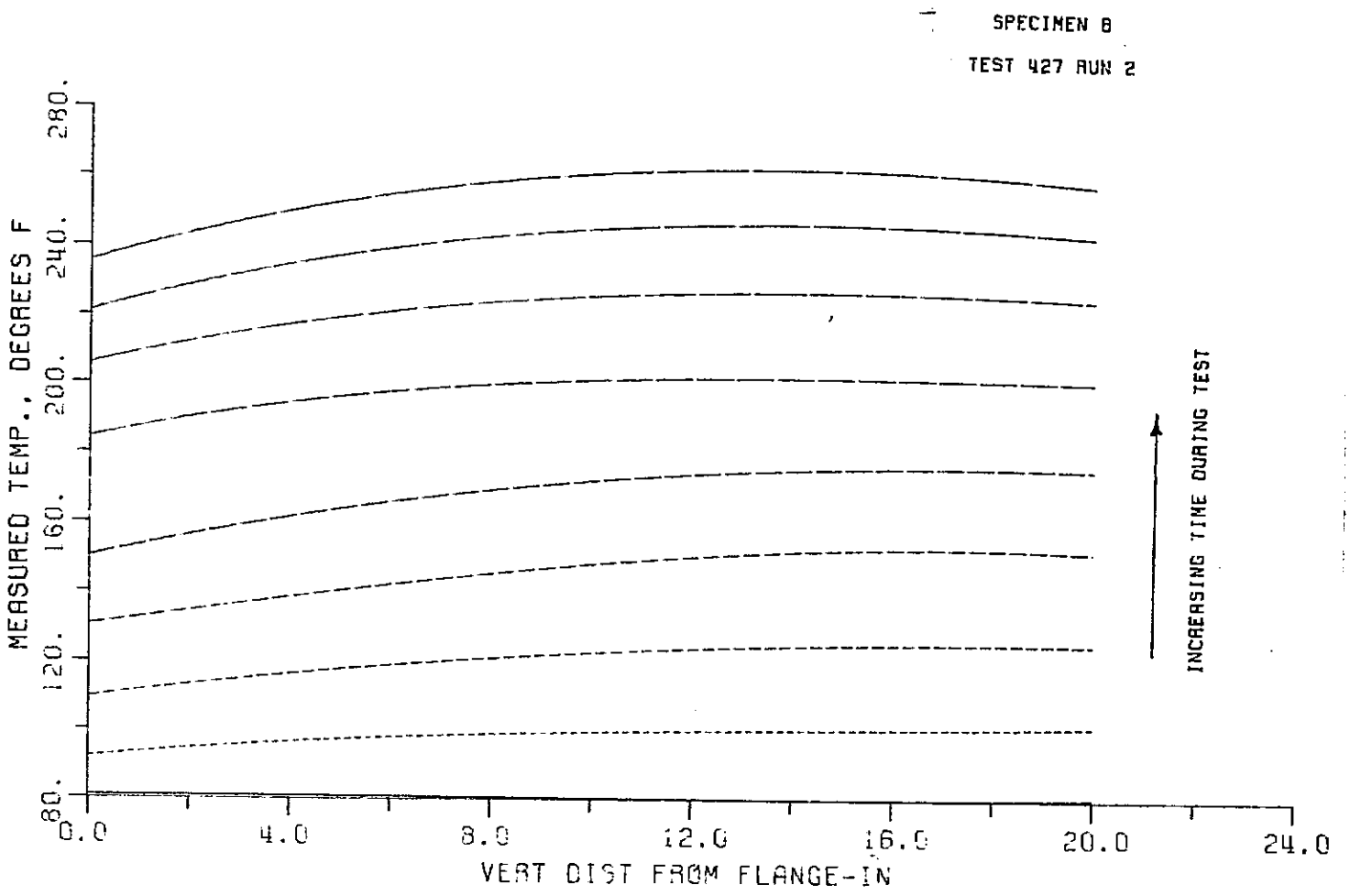

FIGURE 18
SELECTED TEMPERATURE PROFILES ALONG RAIL HEIGHT AT RAIL MIDLENGTH

used to define the buckling stress. The stress level at which the two lines (one for each strain gage) bifurcate is the buckling stress.

Lateral displacement of the rail upper edge at the specimen midlength is plotted against axial stress for both specimens A and B in Figure 19. The displacement magnitude for specimen A is too limited to be conclusive. Specimen B shows a buckling stress of 11,500 psi. which corresponds to an equivalent temperature rise of 88.5°F. Note that the maximum center deflection slightly exceeds 0.75 inch, measured from the undeflected rail centerline to the deflected rail centerline.

Southwell plots made from the data taken during the buckling tests for specimens A and B are presented in Figure 20. The displacement used for this graph was that of the top edge of the rail at the specimen midlength. Also shown on this graph is the Southwell plot for the initial imperfection test on specimen B which will be discussed in the following section. The data from the buckling test of specimen A is insufficient to allow conclusions to be drawn; however, the data for specimen B shows a buckling stress of 11,400 psi (equivalent temperature rise of 88°F). The intercept on the abscissa for this curve is essentially zero, indicating that negligibly small initial imperfections were present.

Figure 21 presents the strain reversal data for specimen B. This graph shows a buckling stress of 11,400 psi (equivalent temperature rise of 88°F).

The buckling mode shape, which was the same for all tests, was a five half-wave mode, nearly symmetric about the rail midlength. Figure 22 shows lateral deflection data taken on the upper edge of specimen B which defines this shape. A photograph of the actual buckled shape of specimen B is shown in Figure 23.

A graph showing the average longitudinal stress (average of the stress on the two faces of the rail) versus distance along the rail in the vertical and in the horizontal directions is presented in Figures 24 and 25, respectively, for selected magnitudes of rail temperature. Note that the rail stress is reasonably uniform in both the vertical and horizontal directions. The uniformity is better, in fact, than would be expected based on the representative temperature differentials presented in Figures 17 and 18. It is apparent from comparing the longitudinal temperature distribution and the longitudinal stress distribution that the rail slips relative to the base flange attachment. This has the effect of improving the axial stress uniformity.

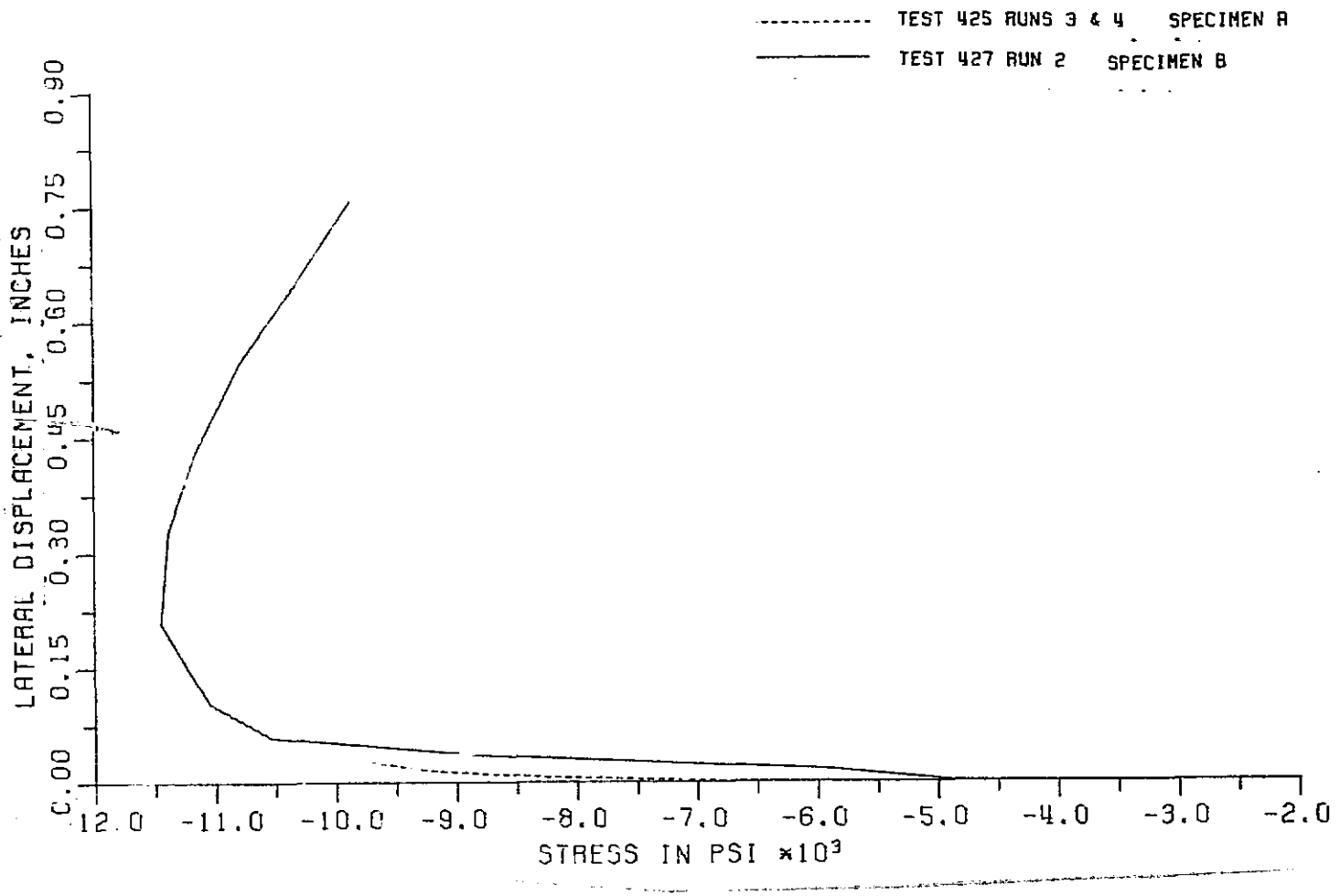

FIGURE 19
LATERAL DISPLACEMENT OF RAIL UPPER EDGE AT SPECIMEN MIDLENGTH VERSUS AXIAL STRESS AT SAME LOCATION

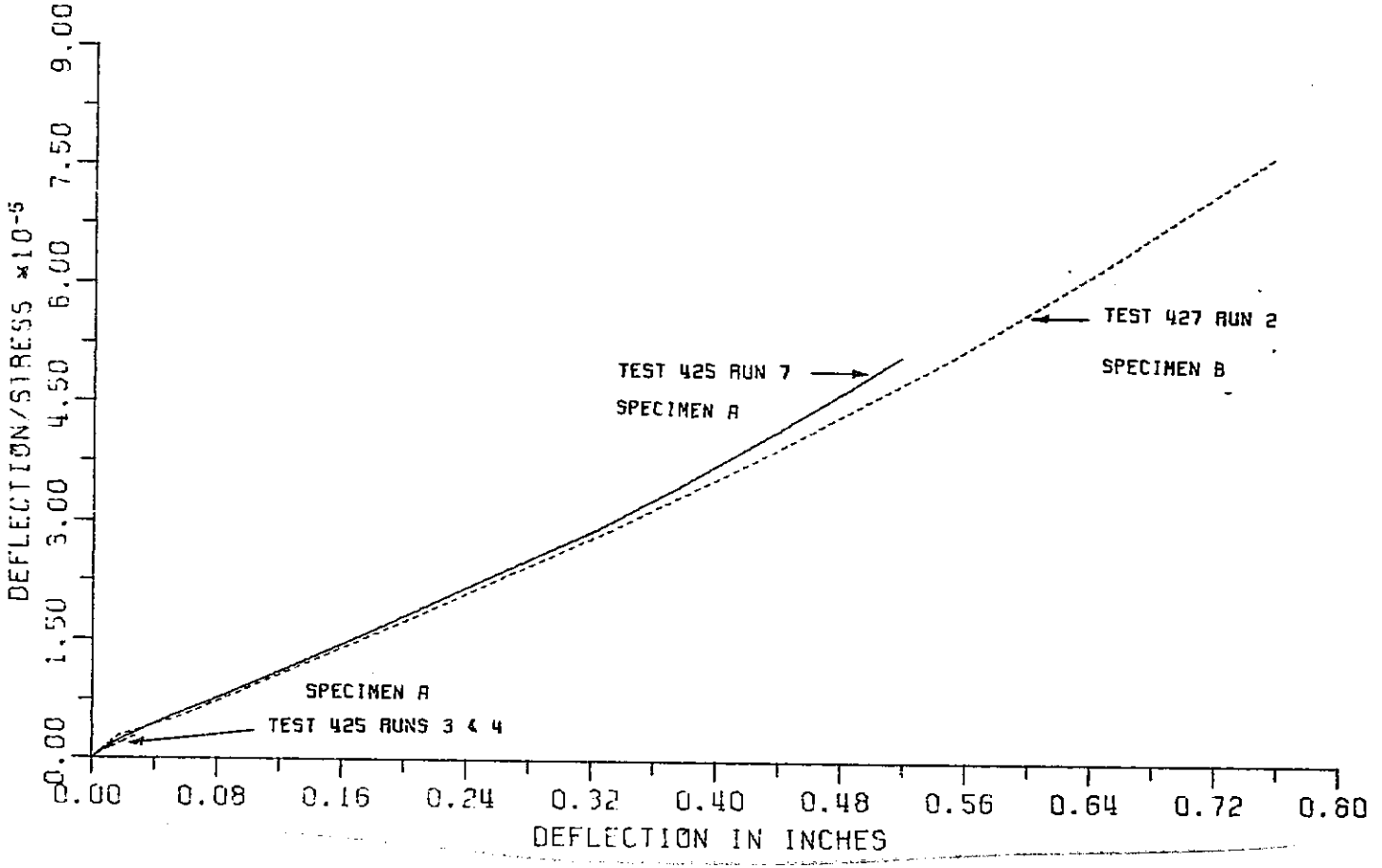

FIGURE 20
SOUTHWELL PLOT

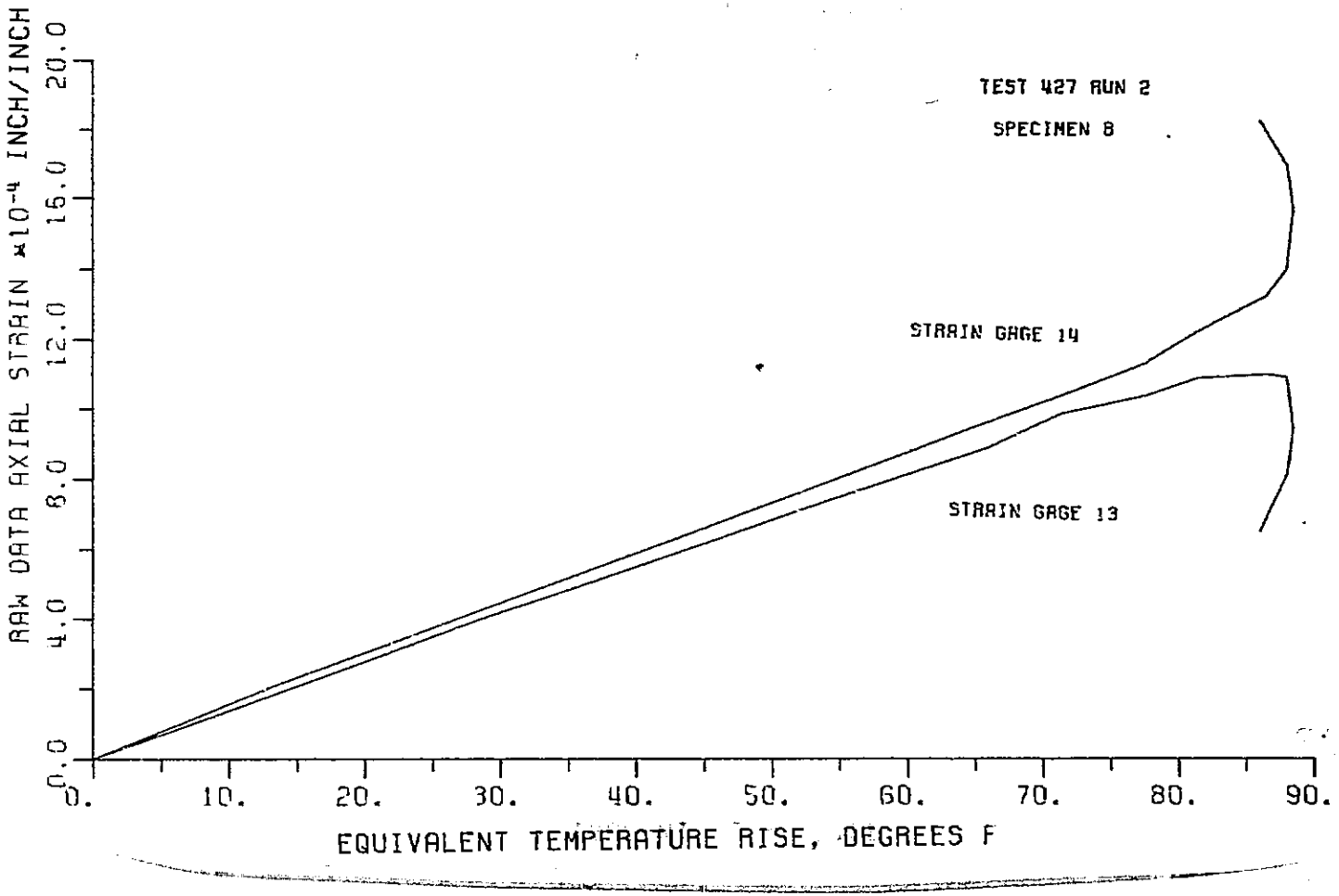

FIGURE 21
STRAIN REVERSAL FOR AXIAL STRAIN GAGES LOCATED NEAR TOP EDGE AT CENTER OF SPECIMEN B

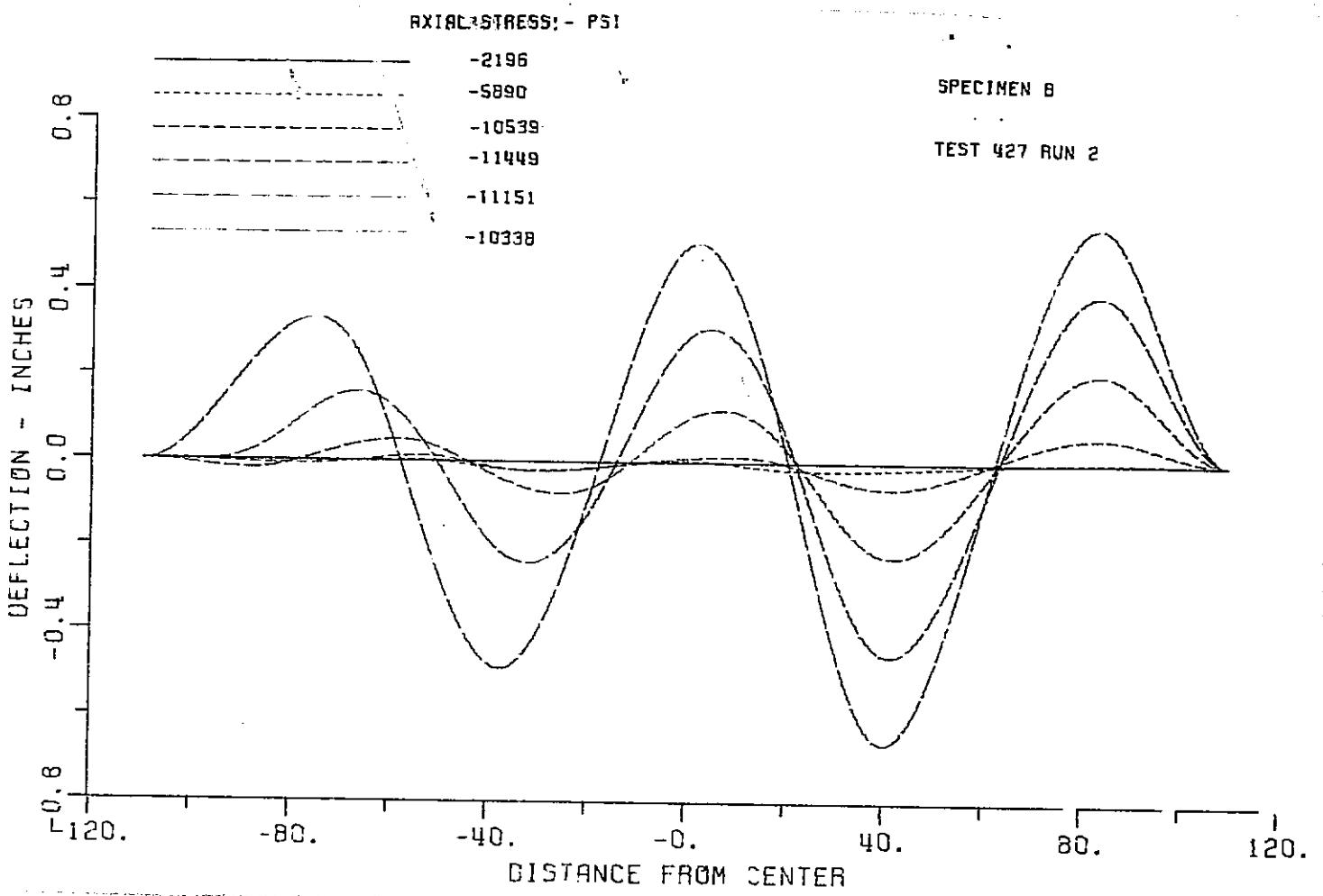

FIGURE 22
LATERAL DEFLECTION OF RAIL UPPER EDGE VERSUS DISTANCE FROM CENTER FOR VARIOUS STRESS LEVELS

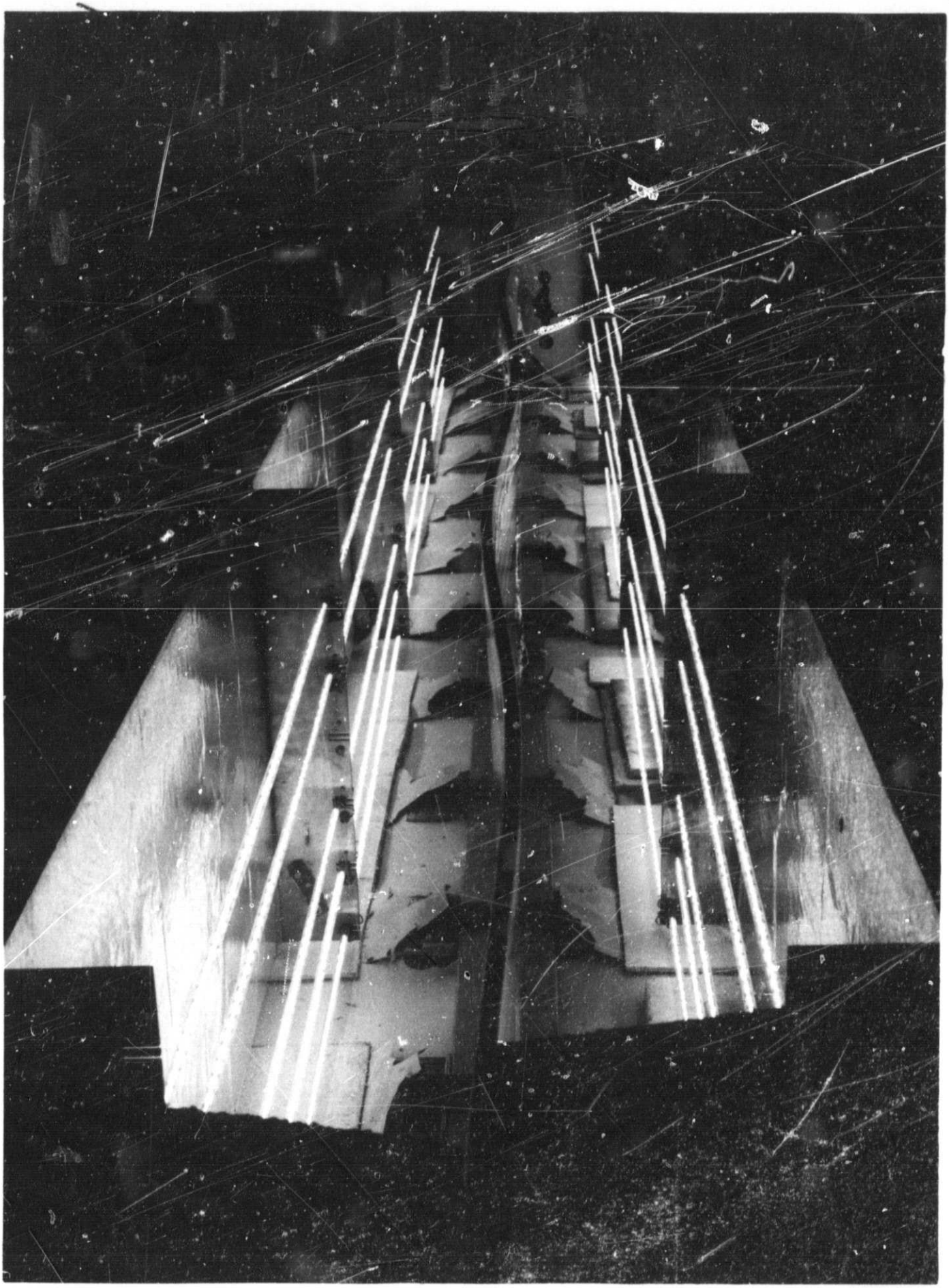

FIGURE 23
BUCKLED RAIL, SPECIMEN B

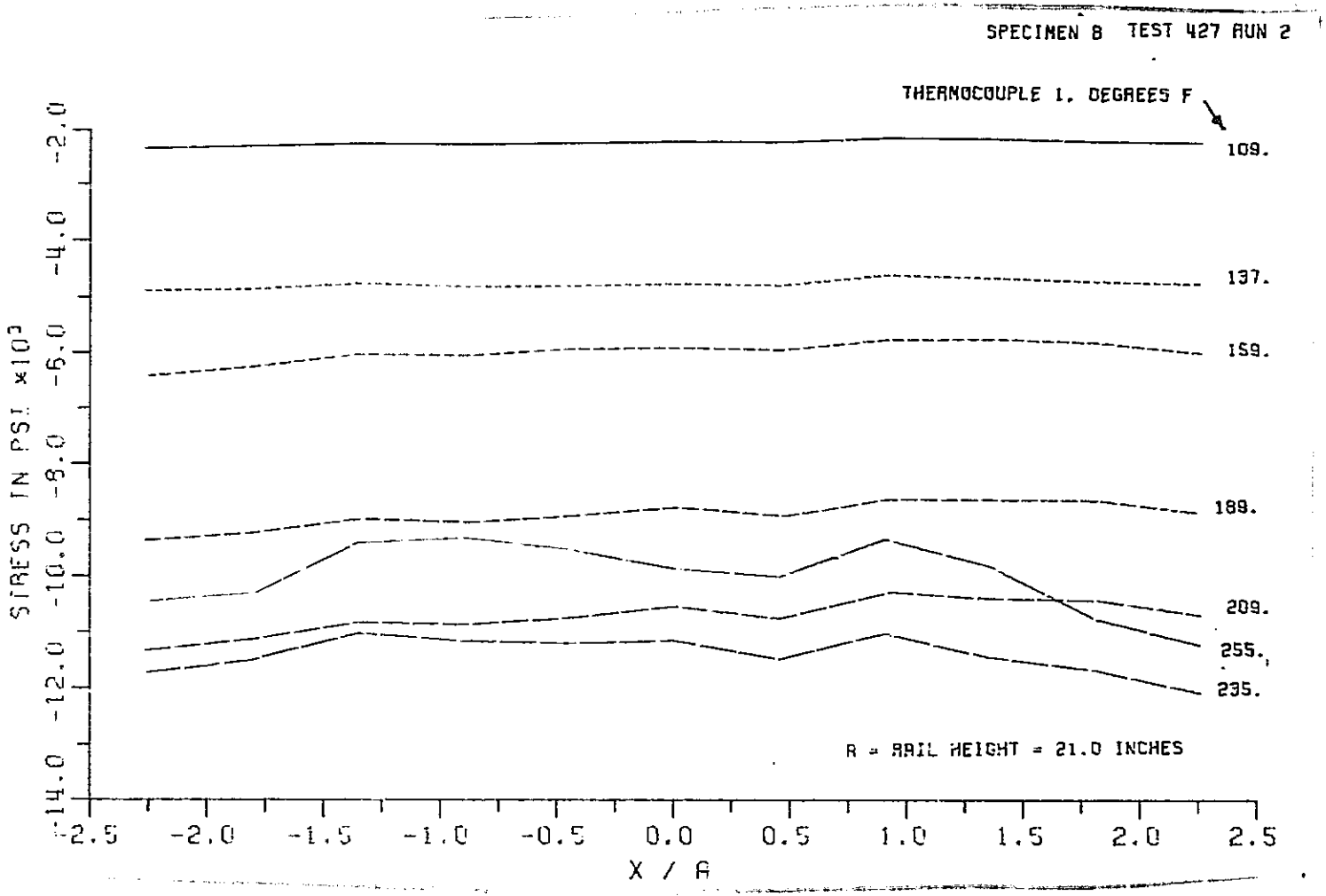

FIGURE 24
AVERAGE OF LONGITUDINAL STRESSES ON TWO FACES OF RAIL
VERSUS DISTANCE FROM CENTER

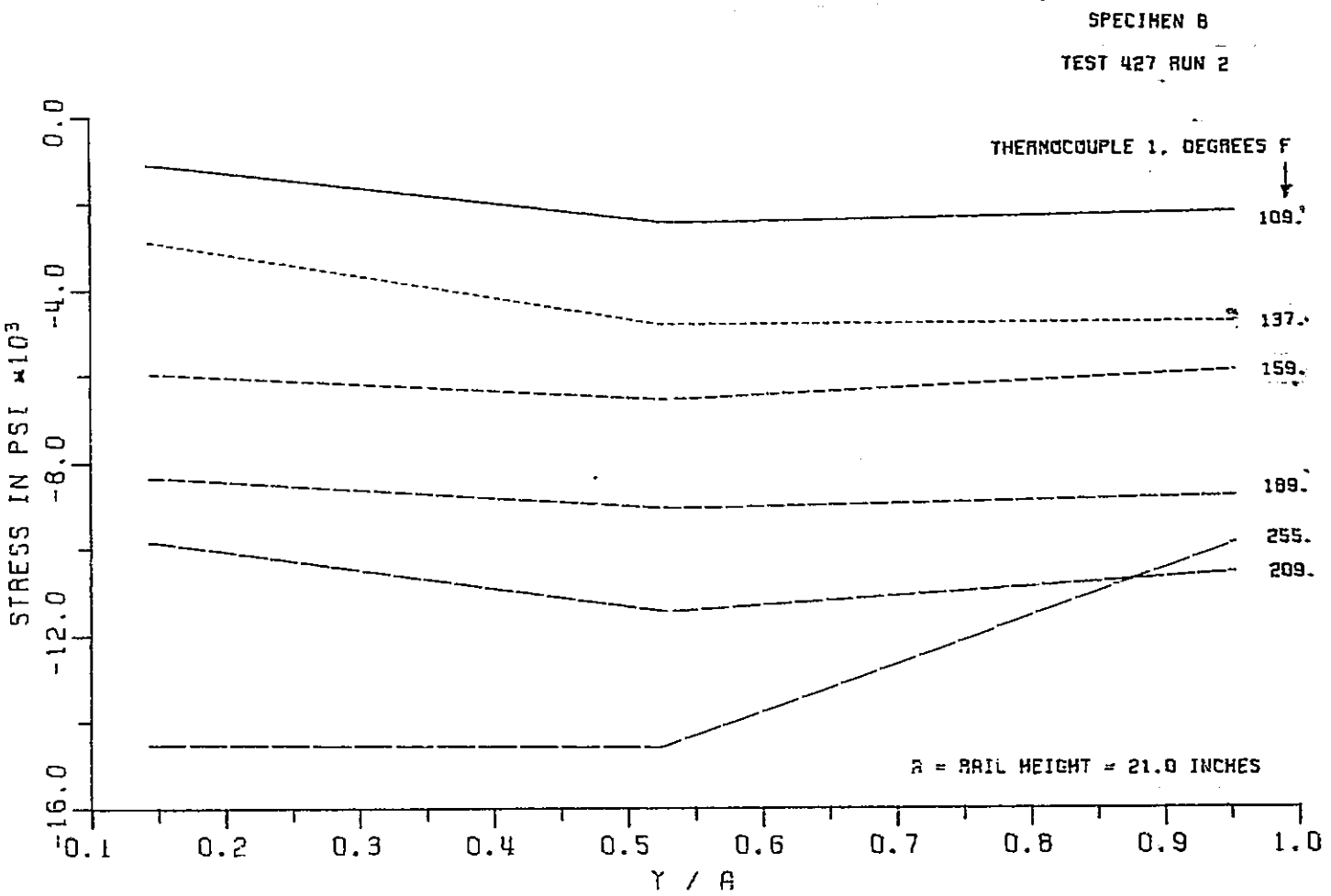

FIGURE 25
AVERAGE OF LONGITUDINAL STRESSES ON EAST AND WEST FACES
OF RAIL AT RAIL CENTER VERSUS RAIL HEIGHT

Figures 19, 24 and 25 show a decrease in the load carrying capability of the upper part of the plate past the buckling stress, a trend which is contrary to that which is typical of supported plates. This can be explained by noting that the above mentioned trend happens only along the unsupported upper edge. Figure 25 shows that the remainder of the rail continues to take stress past the buckling stress value of 11,500 psi compression.

One way to view this behavior is to consider that the free edge of the plate has large deformation post buckling behavior similar to that seen in long columns. This upper edge zone does not carry loads in excess of the buckling stress. However, the remainder of the rail continues to accept load beyond the buckling level because we have chosen to define the buckling stress of the reaction rail on the basis of upper edge behavior alone. A graph similar to Figure 19 but drawn to show lateral deflection of the rail upper edge at specimen midlength versus average longitudinal stress on the rail cross section would show the expected increase in compressive stress past the 11,500 psi buckling load.

INITIAL IMPERFECTION TEST RESULTS

As indicated previously, a sinusoidal initial imperfection with amplitude ±0.1 inch along the rail upper edge and nodes at the rail midlength and at each end was imposed on the specimen in its unloaded configuration. This shape was constructed by inserting shims beneath the tie plates at the proper locations so as to tilt the rail upper edge into the desired shape. Figure 26 shows a plot of the initial imperfection and the subsequent growth of the lateral deformation. Note the transition from the two half-wave initial imperfection to the five half-wave characteristic buckling mode at an equivalent temperature of approximately 80°F. The difference in stress on opposite faces of the rail versus position along the upper edge corresponding to selected magnitudes of equivalent temperature rise is plotted in Figure 27. This stress difference is twice the bending stress at each point. Figure 28 shows the average of the stresses on opposite rail faces. This average is the axial stress along the rail neutral plane. Ideally, this average should be constant along the rail length. In fact, it differs only slightly from a constant.

The data from this test is also shown on the Southwell plot in Figure 20 as Test 425, Run 7. This plot shows that the buckling load is approximately 10,800 psi. (equivalent temperature rise of 84°F). This Southwell plot shows essentially zero initial imperfection since the shape of the initial imperfection used is orthogonal to the actual buckling waveform.

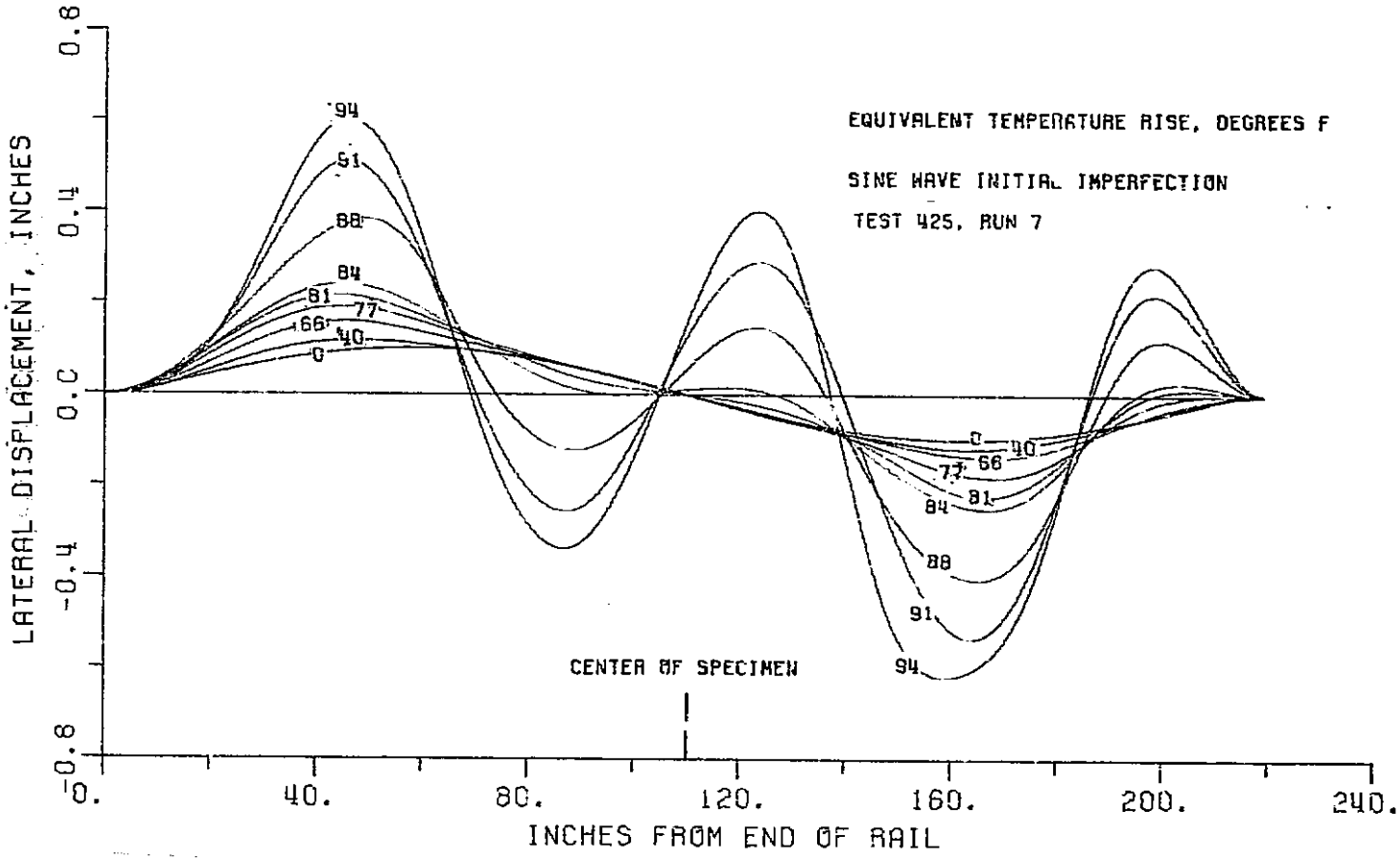

FIGURE 26
INITIAL IMPERFECTION TEST RESULTS FOR SPECIMEN A

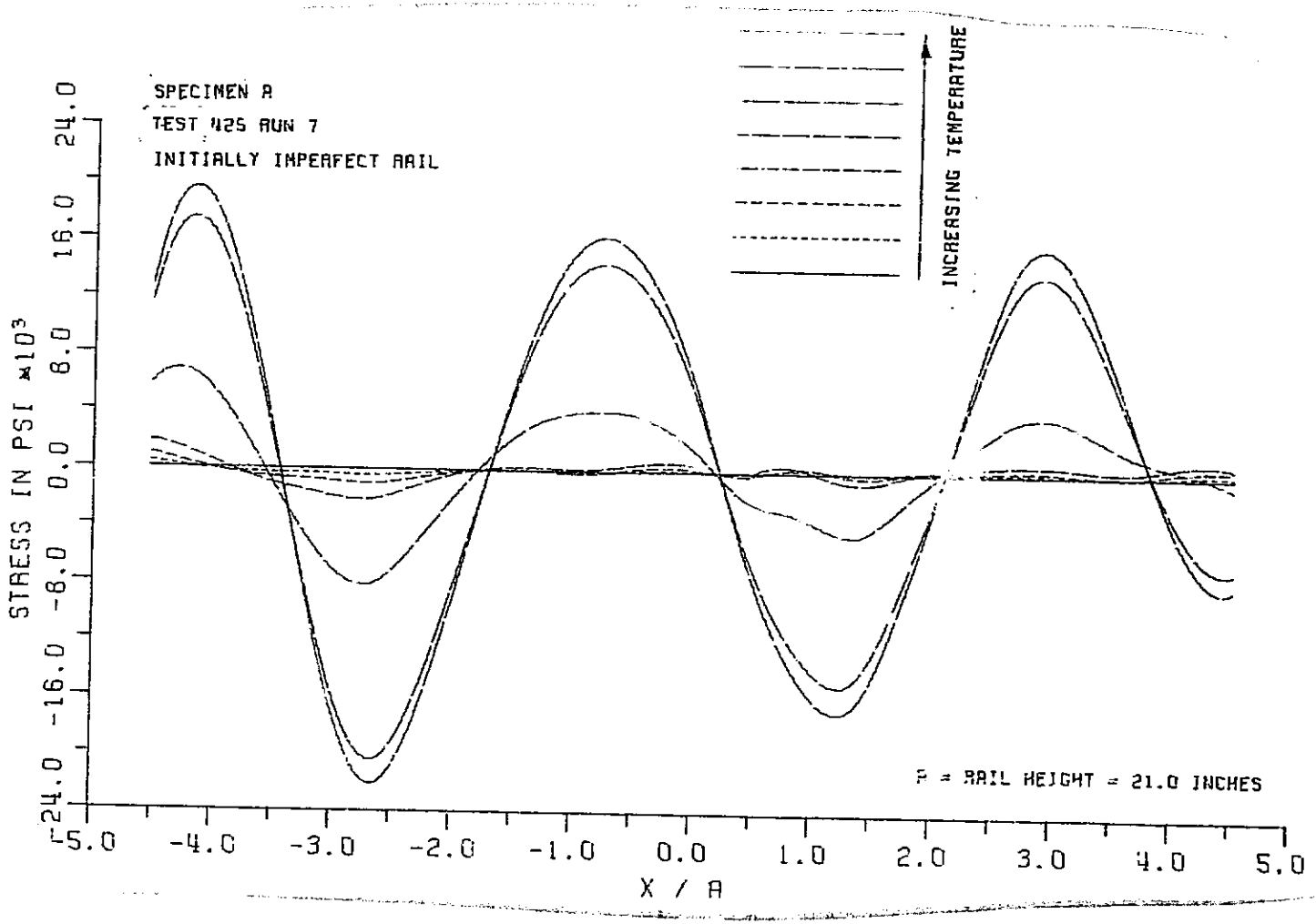

FIGURE 27
DIFFERENCE OF STRESSES ON TWO FACES OF RAIL VERSUS DISTANCE FROM CENTER; INITIAL IMPERFECTION TEST

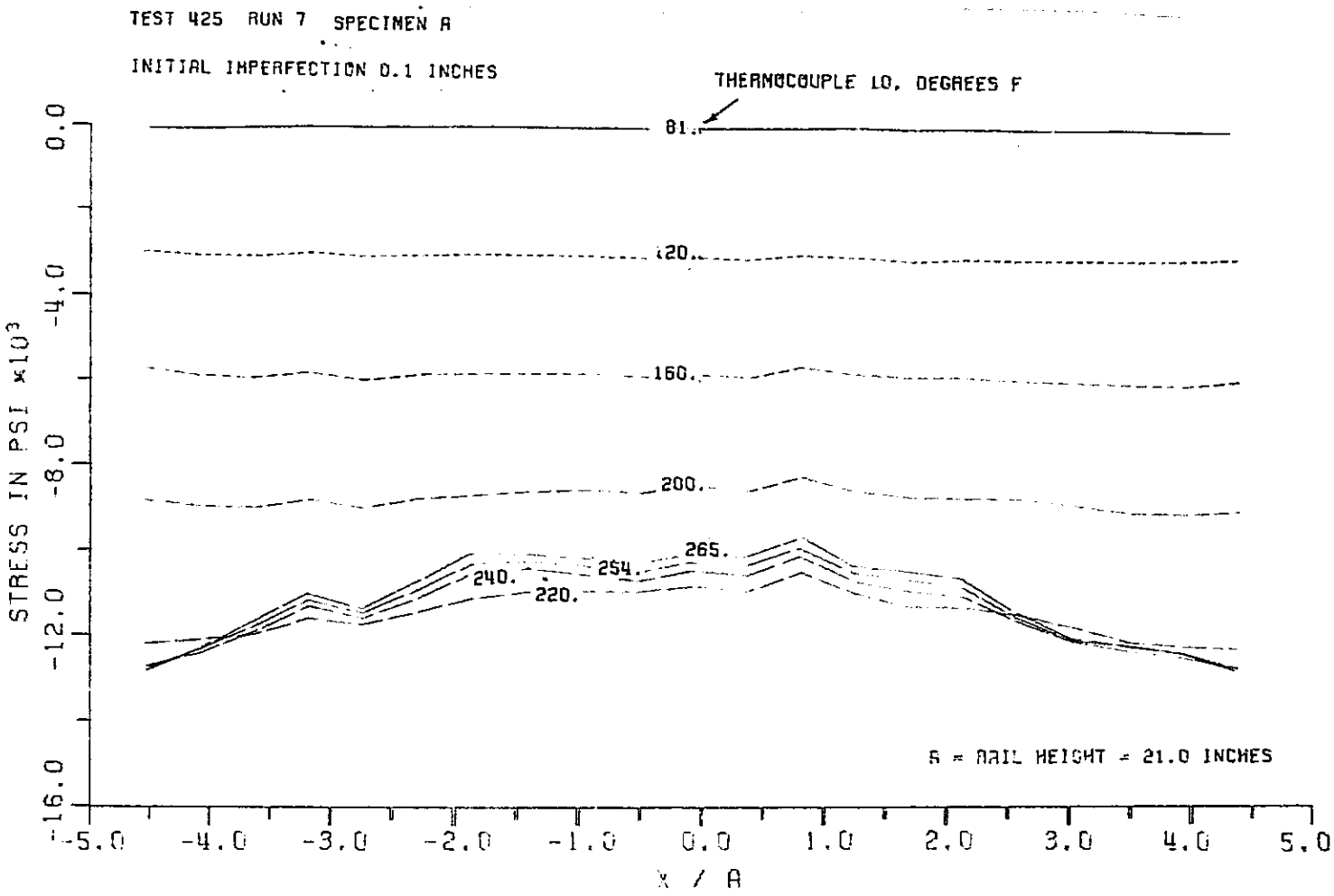

FIGURE 28
AVERAGE OF AXIAL STRESSES ON TWO FACES OF RAIL VERSUS DISTANCE FROM SPECIMEN CENTER; INITIAL IMPERFECTION TEST

The gradual growth of lateral deflections with increasing axial compressive stress is shown in Figure 29. Note that there is only a small increase in axial stress while the deflections grow greatly for axial stress levels over about 10,500 psi compression. This result is also shown in Figure 26, the plot of deflection versus rail length.

LATERAL STIFFNESS TEST RESULTS

The results of the lateral stiffness tests are presented in Figures 30 and 31 which show lateral stiffness versus equivalent temperature rise for specimens A and B, respectively. The data from the two tests is in good agreement and show that the unstressed stiffness value is about 4700 lb./in. This decreases to about 2200 lb./in. for a 75°F equivalent temperature rise. The scatter of the data at the low stiffness end of these curves gives an indication of the difficulty experienced in taking measurements near the buckling load.

Figure 32 shows the deflected shape of the upper edge of specimen B in the presence of a point lateral load of 1000 lb. located 6 inches below the rail upper edge at the specimen midlength. Note that the deflection has decreased to zero at a distance of about three plate heights from the point load.

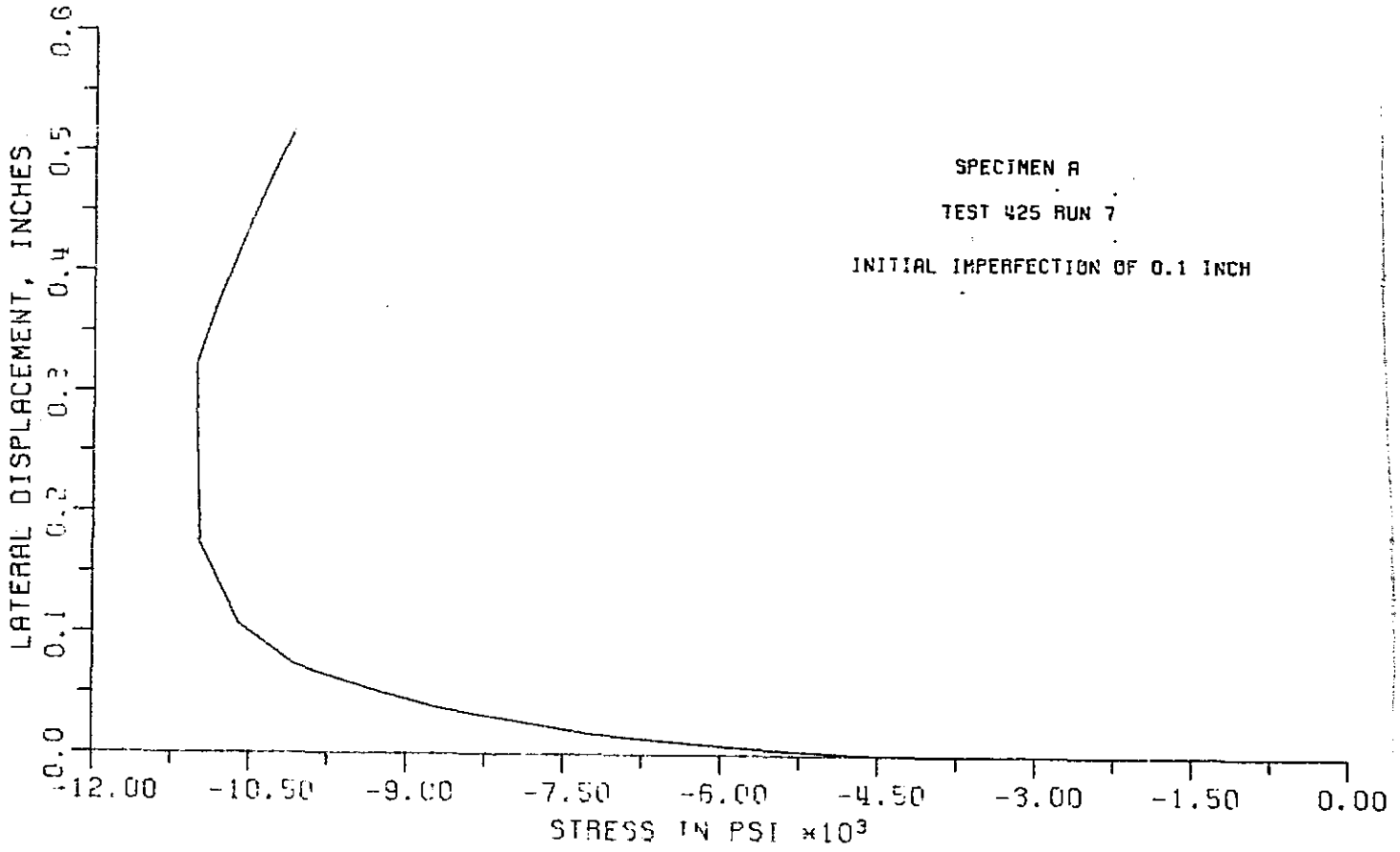

FIGURE 29
DEFLECTION AT RAIL UPPER EDGE AT MIDLENGTH VERSUS AXIAL STRESS; INITIAL IMPERFECTION TEST

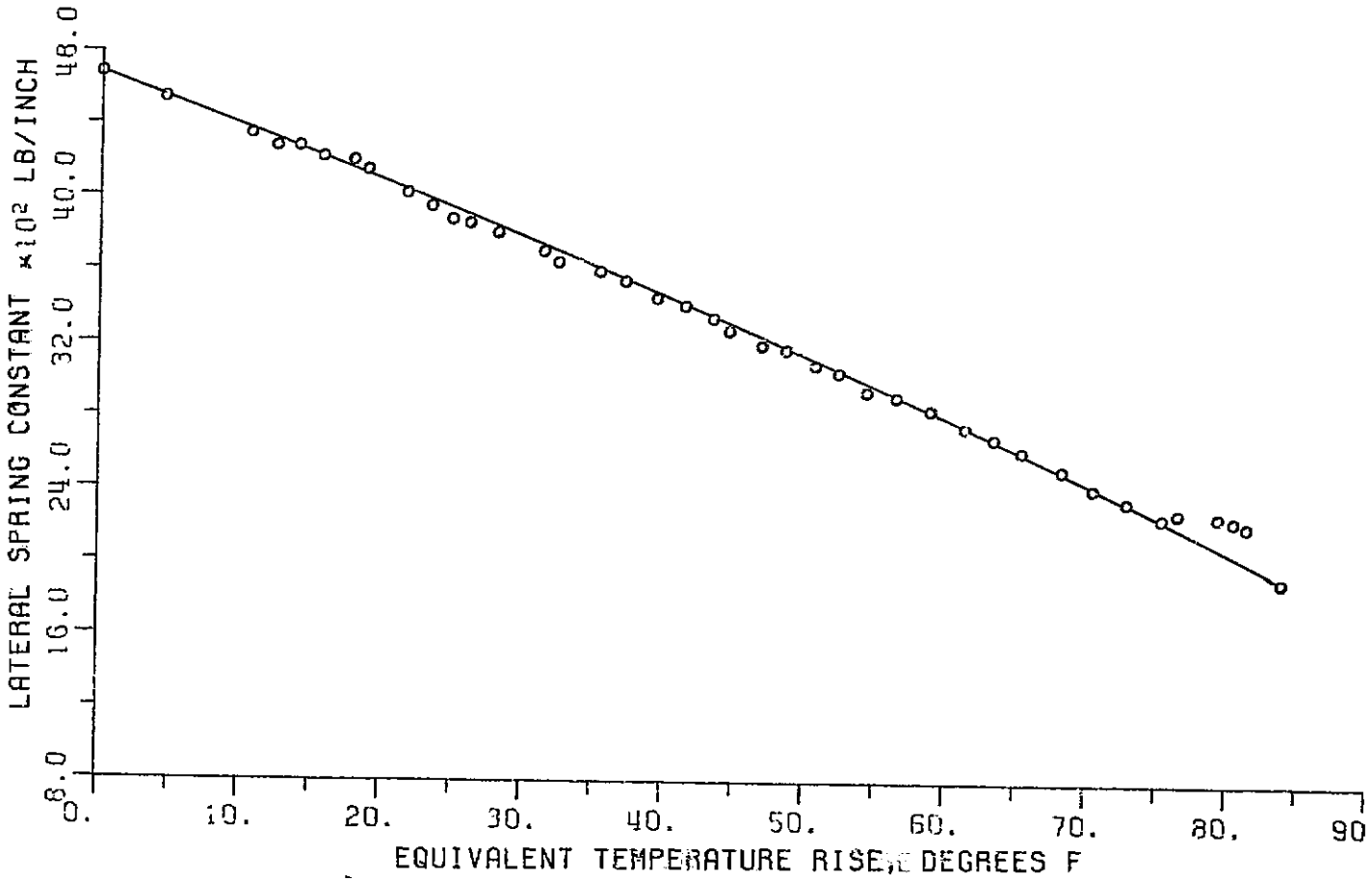

FIGURE 30
VARIATION OF SPRING CONSTANT WITH RAIL EQUIVALENT TEMPERATURE RISE, SPECIMEN A

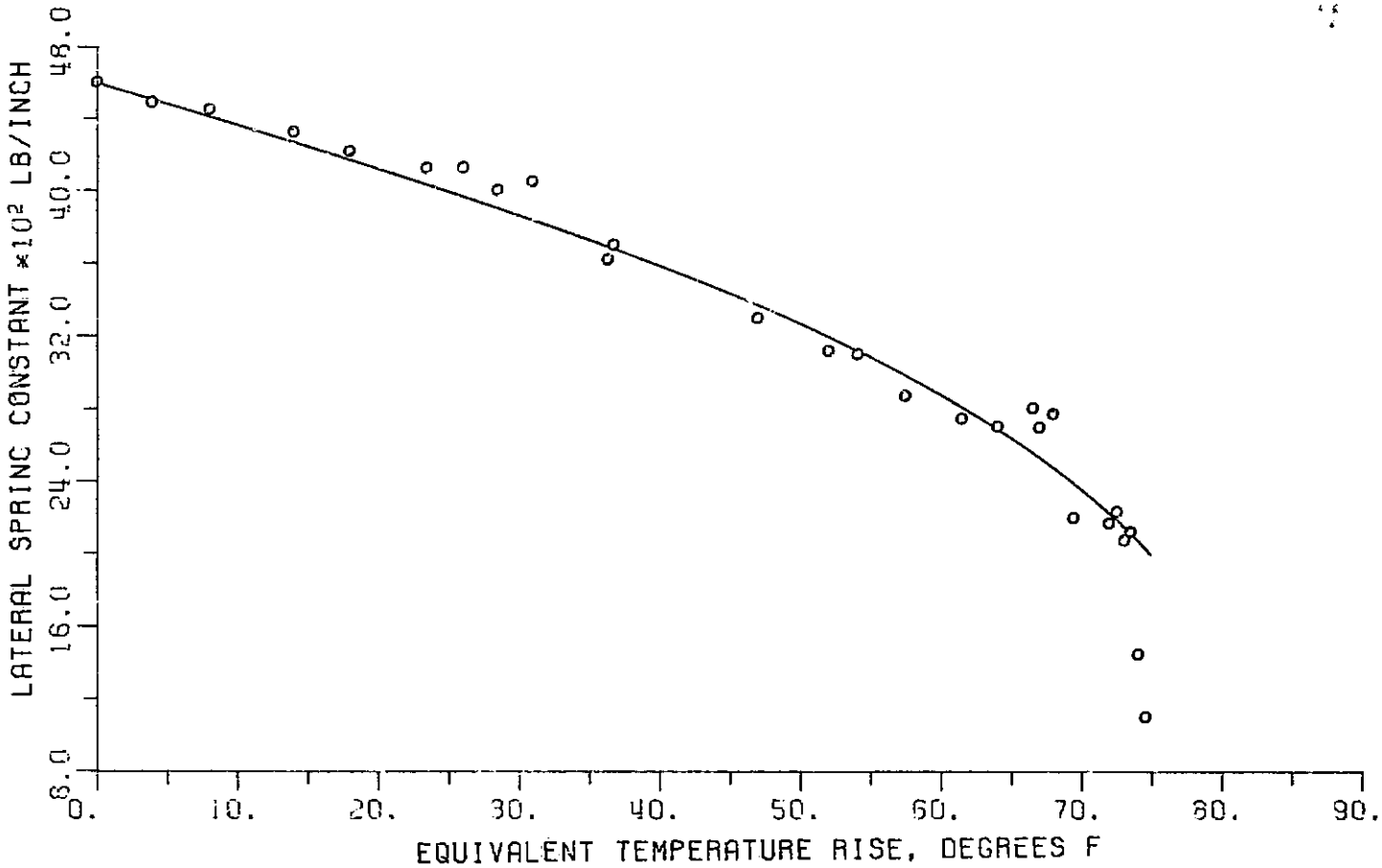

FIGURE 31
VARIATION OF EFFECTIVE SPRING CONSTANT WITH RAIL EQUIVALENT TEMPERATURE RISE, SPECIMEN B

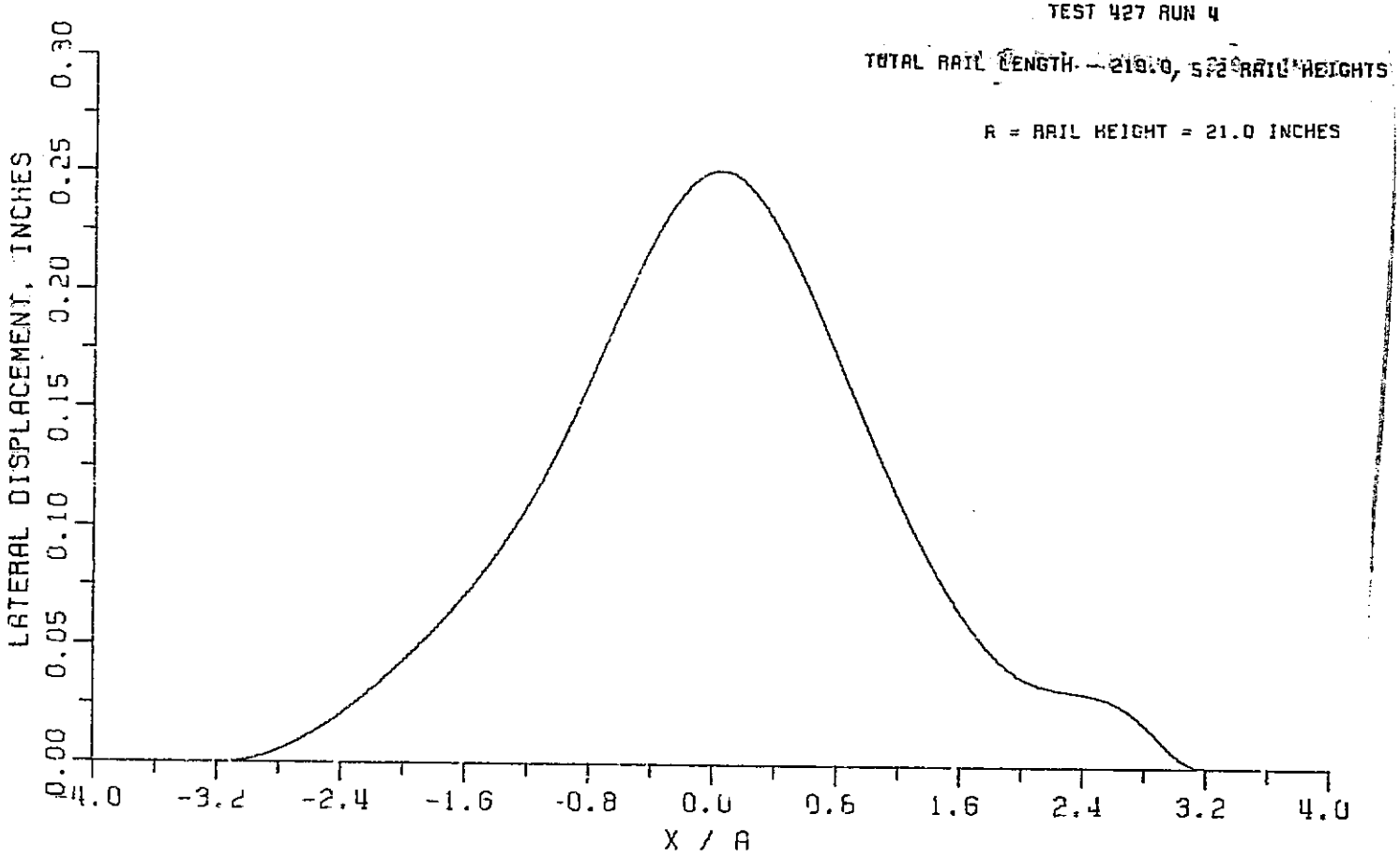

FIGURE 32
UPPER EDGE DEFLECTION UNDER POINT LOAD VERSUS DISTANCE
FROM CENTER FOR A LATERAL LOAD OF 1000 POUNDS

SECTION VIII
CONCLUSIONS

Analysis of the results in the preceding section leads to several conclusions which contribute to the overall understanding of the mechanical behavior of linear induction motor vertical reaction rails and have practical implications for the present installation at Pueblo. These conclusions are:

1. Compressive loads have a less serious effect on the rail static behavior than was generally believed when the original installation was designed. The value of the buckling stress for the "perfect" rail is 10,500 to 11,500 psi. This corresponds to an equivalent temperature rise of 81 to 89°F. Snap buckling, of the type that occurs for long, slender columns, does not occur, even for the "perfect" rail. In the tests, both the "perfect" and initially imperfect rails displayed progressive lateral deflection growth as compressive load increased. The imperfect specimen tested had less than a 50% growth in amplitude of the irregularity until the end load exceeded 90% of the buckling value for a perfect rail. For the initial imperfection shape tested, there was little effect on the buckling load or the rate of growth of lateral deformation with axial stress.
2. Buckling of the rail when it occurs is elastic for amplitudes up to 0.75 inch. The specimens recovered fully from all but the initial irregularities upon removal of the load. The significance of this result is that the installation can now be designed to allow elastic buckling to occur, provided the vehicle is not operated at the time buckling occurs. The buckled rail will return to normal when the temperature decreases.
3. The lateral stiffness of the rail declines gradually for increasing compressive load. At zero stress, the stiffness is about 4700 lb./in.; it decreases to about 2300 lb./in. at 10,000 psi compressive stress. A good linear approximation to the stiffness function is that it drops off at a rate of 30 lb./in. per °F of rail temperature increase.
4. The half wavelength of the buckling mode for this reaction rail is approximately 38 inches. Since the length of the test specimen was chosen sufficiently long, this wavelength should not be significantly different for the long continuous

rail in the field. One conclusion based upon knowledge of the buckled wavelength is that the most serious kind of initial irregularity is one which is periodic with a half wavelength of 38 inches.

SECTION IX
RECOMMENDATIONS FOR AN IMPROVED FIELD INSTALLATION

The results of this test program clearly show that a field installation prestressed so that no compressive stress is generated for any probable rail temperature is overly restrictive. The experiments show that substantial axial loads can be generated without causing significant lateral deformation, even for a rail with initial lateral irregularities. Furthermore, buckling deformations up to 0.75 inch are elastic and disappear upon reduction of the axial load. These conclusions lead to a recommendation for an improved field installation which does not require any redesigned hardware.

The suggested improved installation results in a lower tensile stress at low rail temperatures by reducing the installation temperature of the rail. Figure 33 shows axial stress plotted against rail temperature. The uppermost diagonal line represents the original field installation as installed at 140°F. Note that the tensile stress is zero at 140°F and 22,000 psi at -30°F. The recommended installation fixes the stress-free temperature at 80°F which causes the tensile stress at -30°F to be 14,500 psi and the compressive stress at 140°F to be 7,800 psi. The latter stress is approximately 78% of the buckling stress; at that level the lateral stiffness is approximately 2800 lb./in. Reference to the graph of deflection versus stress for the initially imperfect rail (Figure 29) shows that at 7800 psi compression the growth in the amplitude of the initial imperfection is about 30% of the 0.1 inch initial amplitude. For reference, the average tensile strength across welds in the field as shown by Garrett-AiResearch testing is shown in Figure 33.

It may be advisable to limit vehicle operation to times when the rail temperature is below 120°F. This will assure that the size of the lateral deformations arising from compressive forces acting on initial imperfections in the rail will be small during vehicle operation.

An additional constraint on the recommended installation is that the rail lateral stiffness be sufficiently high for adequate guidance of the linear induction motor. At this time, a minimum acceptable rail lateral stiffness value has not been determined. However, preliminary informal communications with the vehicle prime contractor indicate that a value of 3000 lb./in. is satisfactory for vehicle operation.

It should be emphasized that the recommendations made in this report are based upon static considerations alone. The dynamic response of the vehicle or the rail may be affected by high speed operation in the presence of substantial compressive loads.

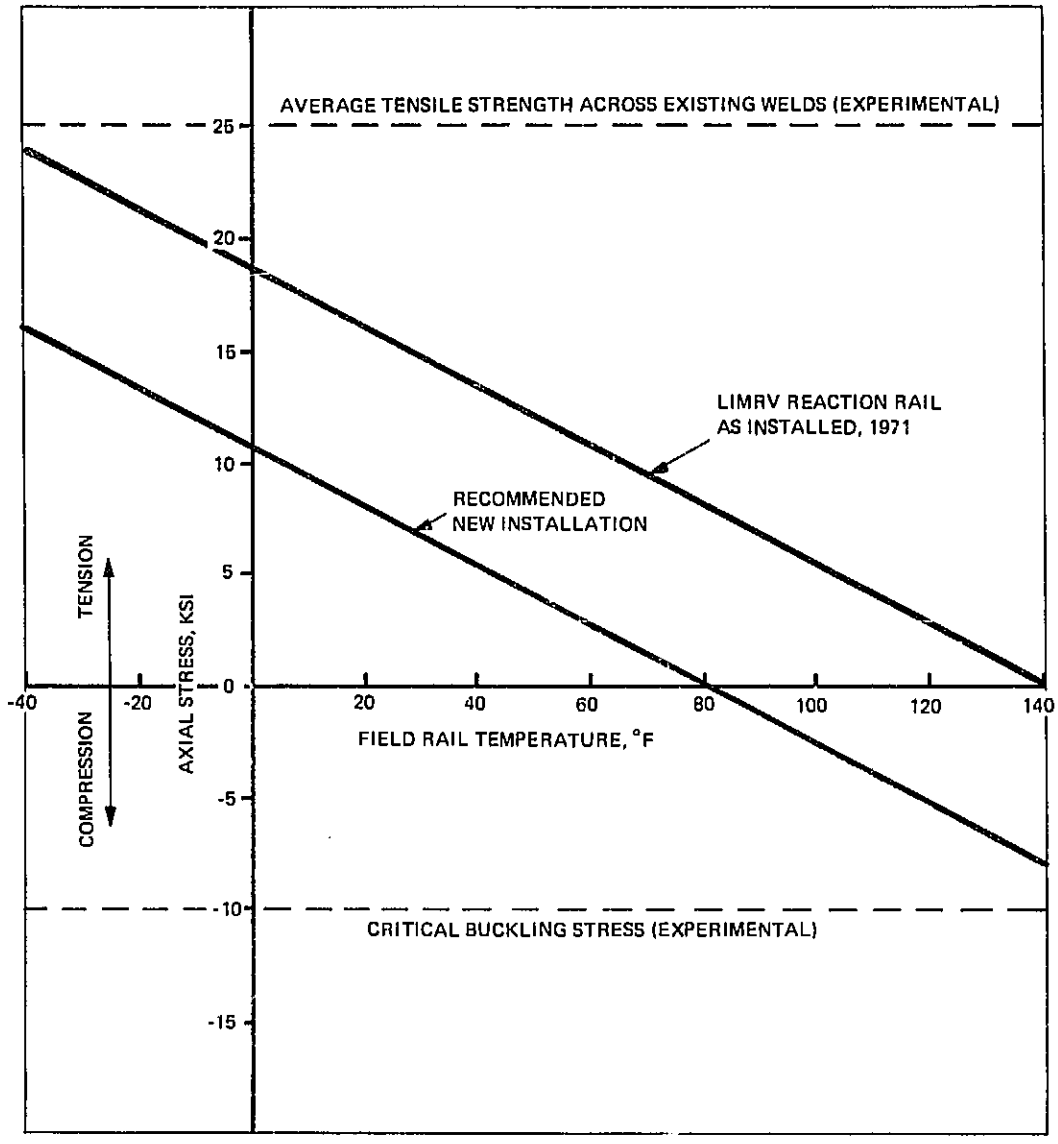

FIGURE 33
AXIAL STRESS VERSUS FIELD RAIL TEMPERATURE

APPENDIX I
TESTS ON THE RAIL BASE ATTACHMENT HARDWARE

The displacement response of the base flange attachment system to loading was experimentally measured by applying either a horizontal or vertical force and measuring the corresponding rail and attachment displacements. An equivalent horizontal or vertical spring constant for each tie plate attachment system was defined as the load necessary to obtain a unit displacement response in the horizontal or vertical directions, respectively. Factors which influence these equivalent spring constants, in addition to the elastic properties of the tie clip, include the crosstie and subgrade flexibility and the displacement of the lag bolts relative to the wood crossties.

Vertical Equivalent Spring Constant—The experimental setup used to measure the equivalent vertical spring constant is shown in Figure AI-1. The setup permitted a measurement of the influence of the tie clip and lag bolt attachment flexibility, but did not include the effect of crosstie and subgrade flexibility. A short section of the wooden crosstie was attached rigidly to the lower platen of a 120,000 pound capacity hydraulic test machine. A short section of rail was attached to the crosstie using a typical single tie plate, clip, and lag bolt system installed as described in Appendix III. The upper edge of the rail was gripped by the upper crosshead platen. The upper platen was displaced relative to the lower platen, thus imposing an upward load on the tie clips and lag bolts. It was found that this loading caused the tie clip to deform such that it was in contact with the rail only along a line at the outer edge of the rail base flange and that this line contact was maintained as the specimen was loaded. The tie clip and base plate displacements were electronically measured as a function of the applied load using a linear voltage displacement transformer (LVDT).

The vertical displacements of two points were monitored in these tests. The position of the first point was directly over the line of contact between the tie clip and the rail flange at the center of the clip. The second point was a point on the tie plate adjacent to the tie clip. The displacements of the second point were subtracted from the displacements of the first point to provide an accurate indication of the vertical spring constant of the clip and lag bolt system.

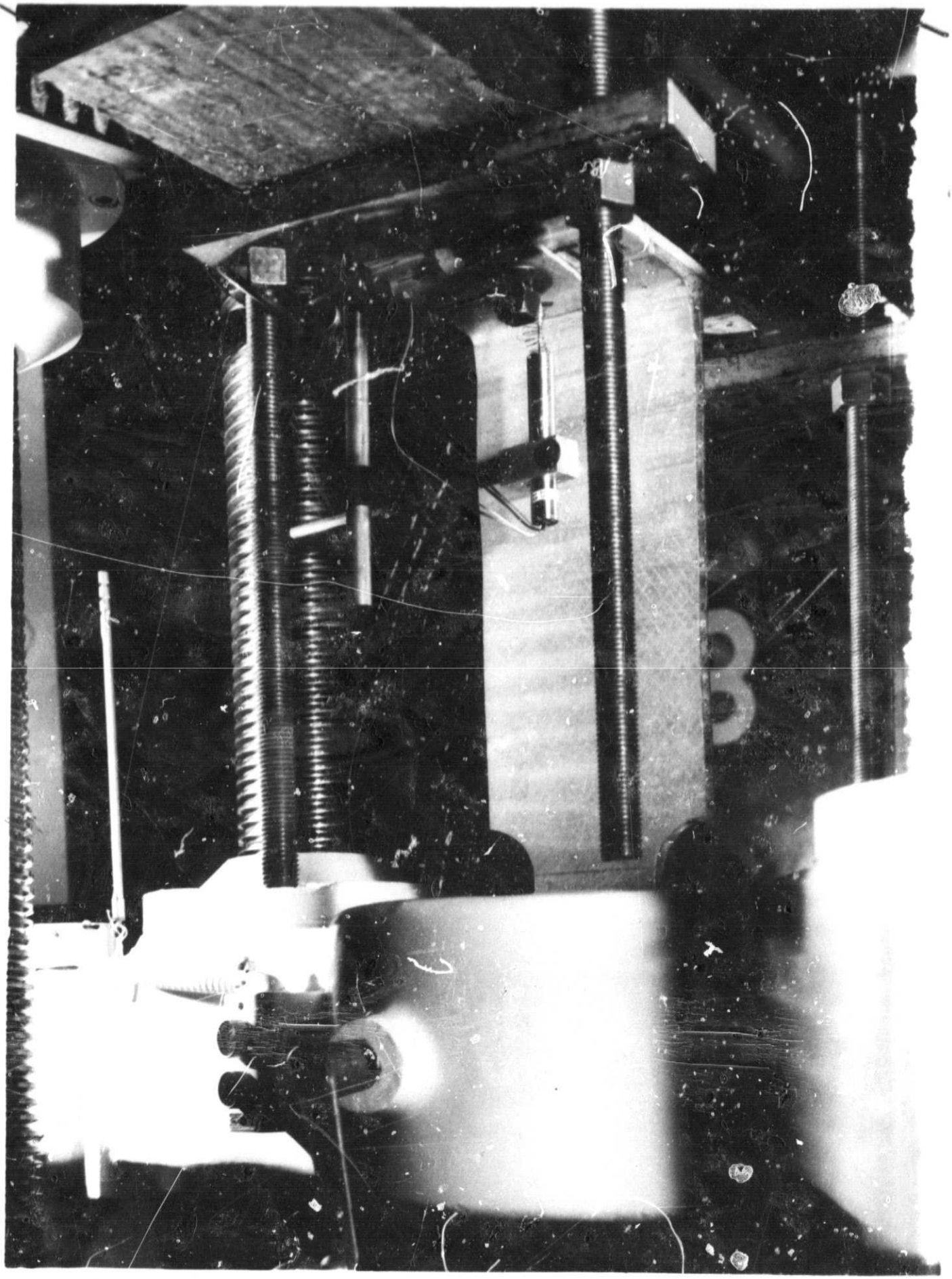

FIGURE AI-1
VERTICAL EQUIVALENT SPRING CONSTANT TEST SETUP

The results of these measurements plotted versus the applied load is presented in Figure AI-2. Four different curves are plotted in the figure and represent tests in which: (1) no lateral shims were placed in the gap between the tie plate and the rail; (2) lateral shims were symmetrically installed (half of the shims on each side of the rail); (3) lateral shims were installed with all of the shims on one side of the rail with displacements measured on the same side; and (4) lateral shims were installed with all of the shims on one side of the rail with displacements measured on the opposite side. Very little difference is indicated between results for symmetric shims, no shims, and all of the shims located on one side with displacements measured on the opposite side. A significant reduction, however, occurs when all of the shims are located on one side of the rail and when displacements are measured on the same side. This is due to the increase in the tie clip cantilever moment arm. The effective vertical spring constant per tie clip based on the initial slopes for symmetric shims, and shims located on one side only with displacements measured on this same side, are 2.5×10^6 pounds per inch and 0.43×10^6 pounds per inch per tie clip, respectively.

Horizontal Equivalent Spring Constant—The experimental setup used to measure the horizontal equivalent spring constant is presented in the photograph of Figure AI-3. This arrangement measures the response of subgrade and crosstie flexibility, as well as that of the attachment system. A section of rail which spans two crossties was attached with two tie plate systems to two wooden crossties. The crossties were affixed to four-inch by four-inch wooden supports which were bolted to the laboratory floor in the same manner as for buckling tests. A lateral load was applied to the rail at the midpoint between crossties and six inches below the rail upper edge. Absolute displacements of the tie plates corresponding to the applied load were recorded using LVDT instruments.

A graph of the lateral load versus tie plate displacements is presented in Figure AI-4. The horizontal equivalent spring constant per tie plate determined as the slope of the initial tangent is 144,000 pounds per inch.

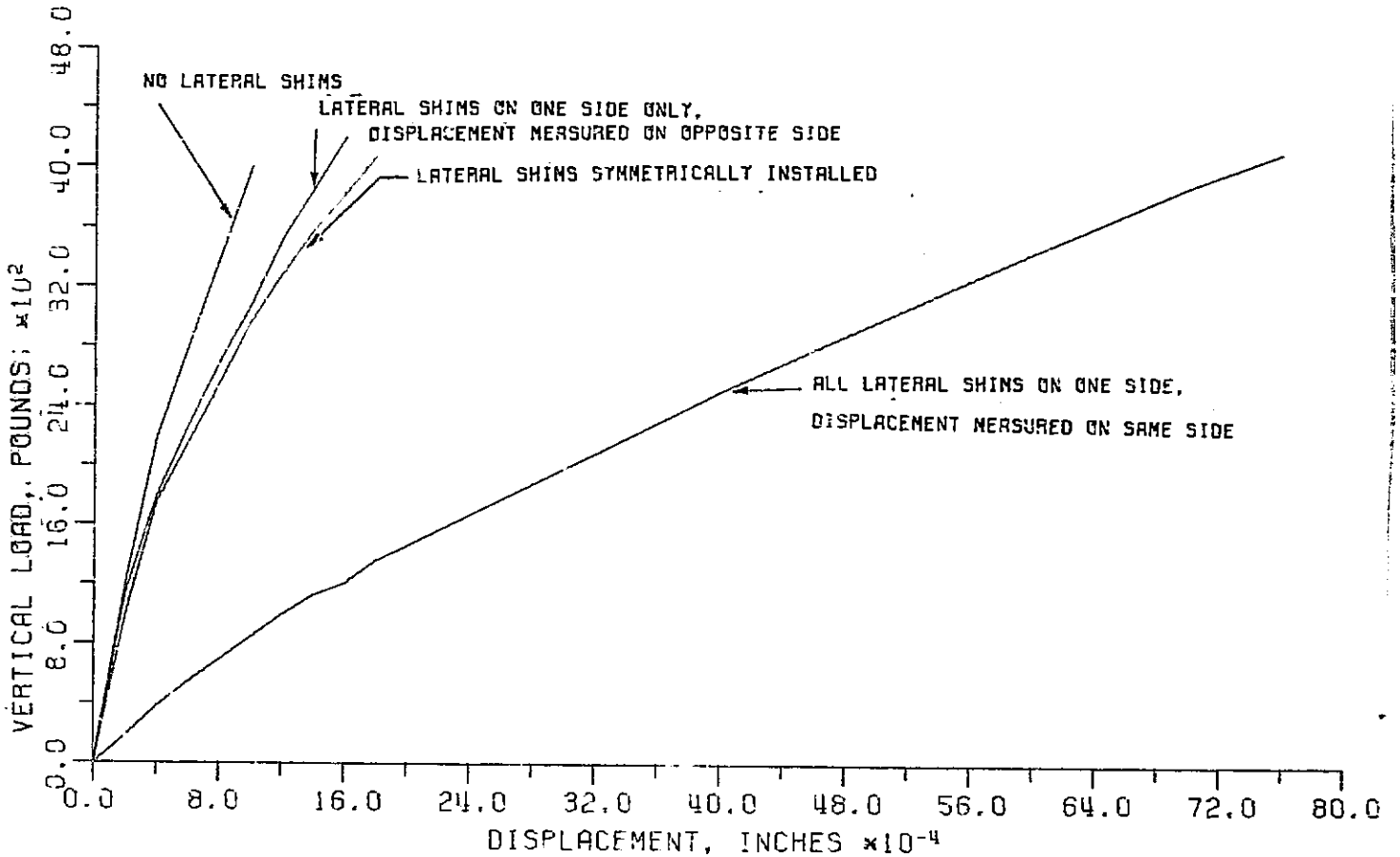

FIGURE AI-2
VERTICAL LOAD VERSUS DISPLACEMENT FOR VARIOUS
HORIZONTAL SHIM ARRANGEMENTS

NASA
L-72-4824

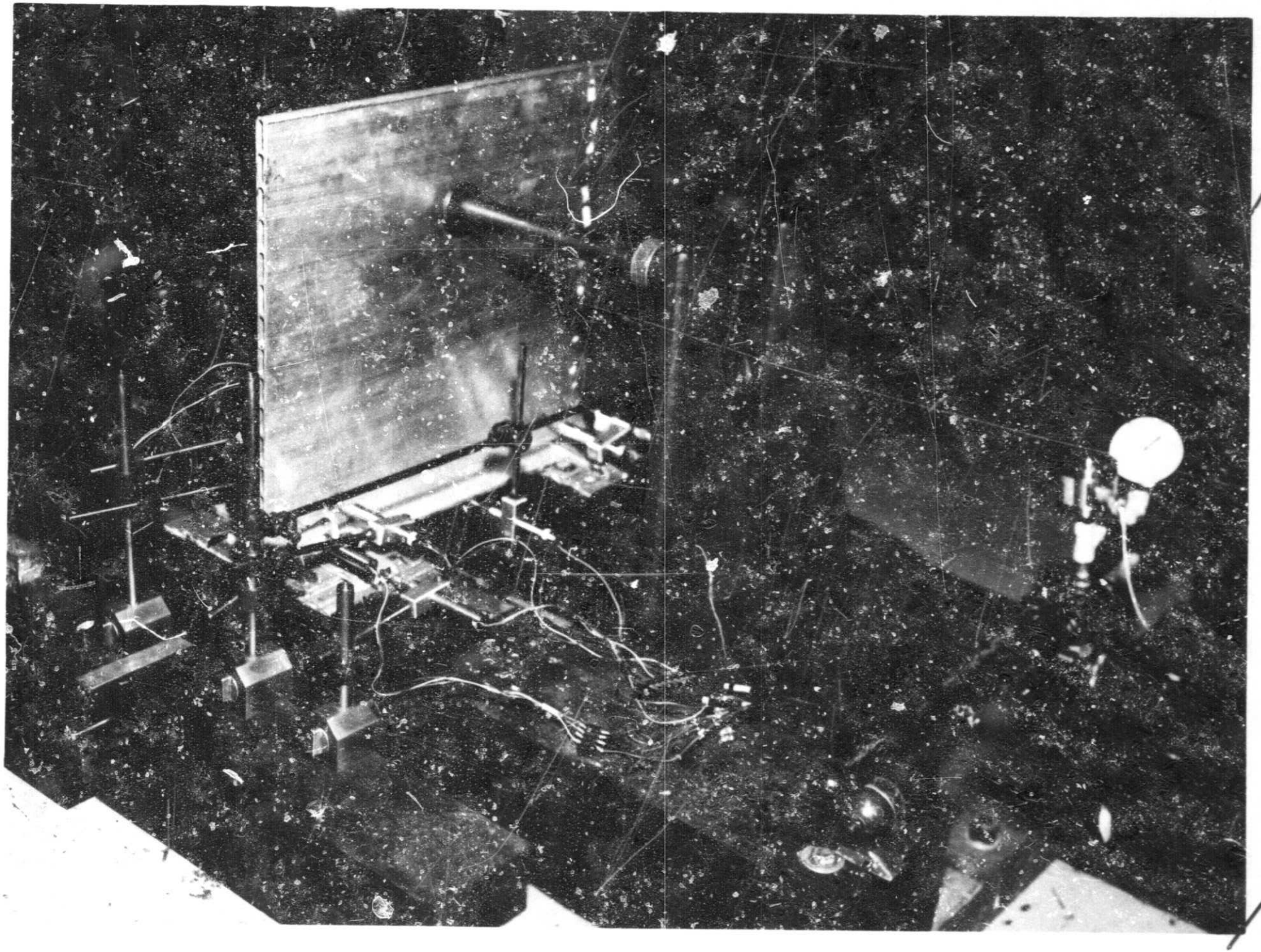

FIGURE AI-3
HORIZONTAL EQUIVALENT SPRING CONSTANT TEST SETUP

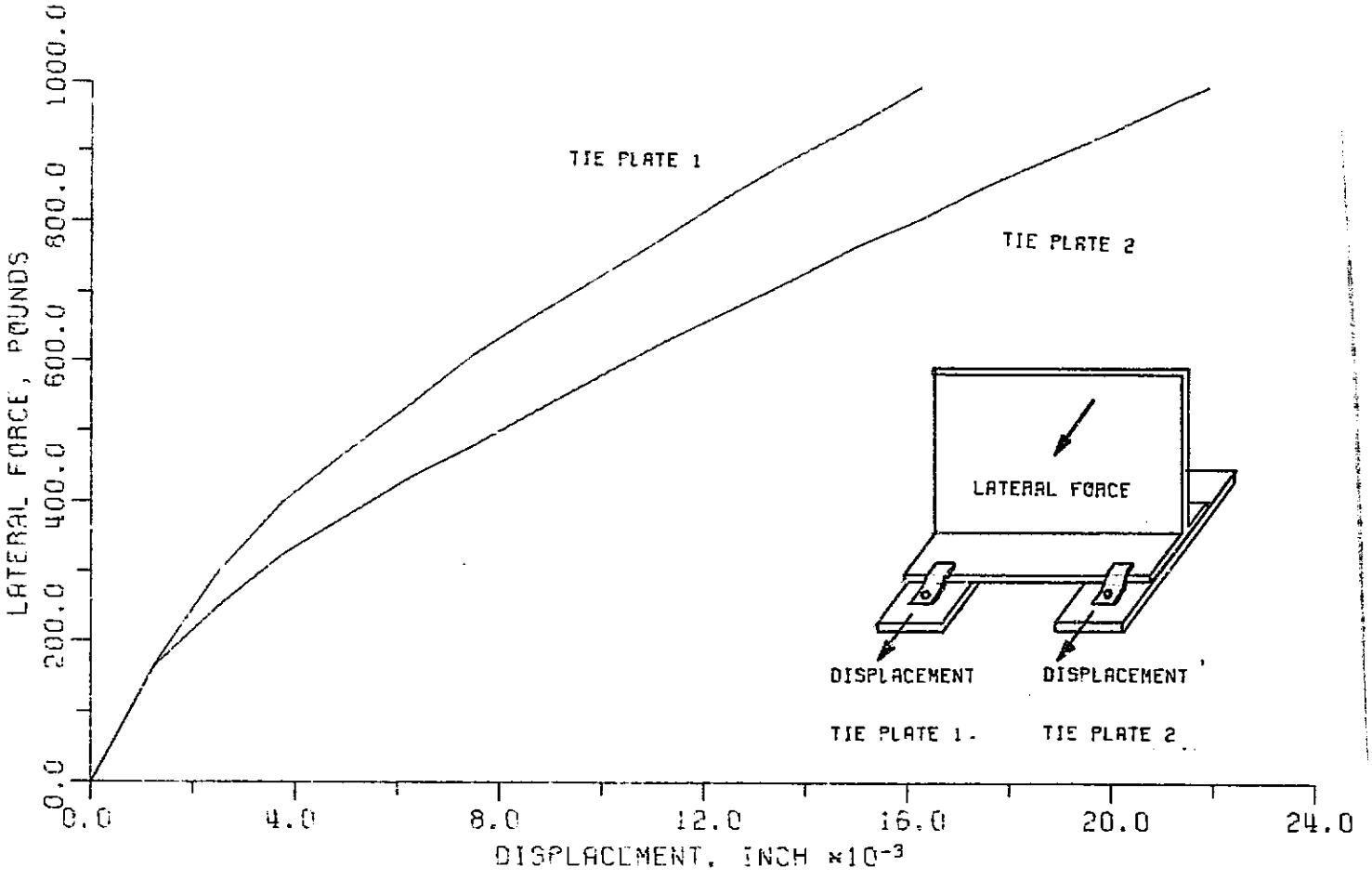

FIGURE AI-4
LATERAL FORCE VERSUS DISPLACEMENT FOR HORIZONTAL
EQUIVALENT SPRING CONSTANT TEST

APPENDIX II
LOCATION OF INSTRUMENTS

This appendix contains diagrams showing the locations and numbering systems for the instruments used in this test series. Figure AII-1 shows the layout of the strain gages used. Circled symbols indicate that the gage appears in a coincident location on the back surface of the rail as well as on the front surface as shown in the diagram. Figure AII-2 shows the thermocouple locations. Again, circled symbols indicate the instrument appears on both front and rear faces of the rail. Specimen B was instrumented so that a map of the vertical and horizontal temperature distributions could be obtained. Figure AII-3 gives the locations of the linear voltage displacement transformers (LVDT's). In this diagram, some instrument numbers appear more than once on the same specimen. This indicates that the sensor was moved from one location to the other during testing of that specimen. All LVDTs were attached to the same face of the rail.

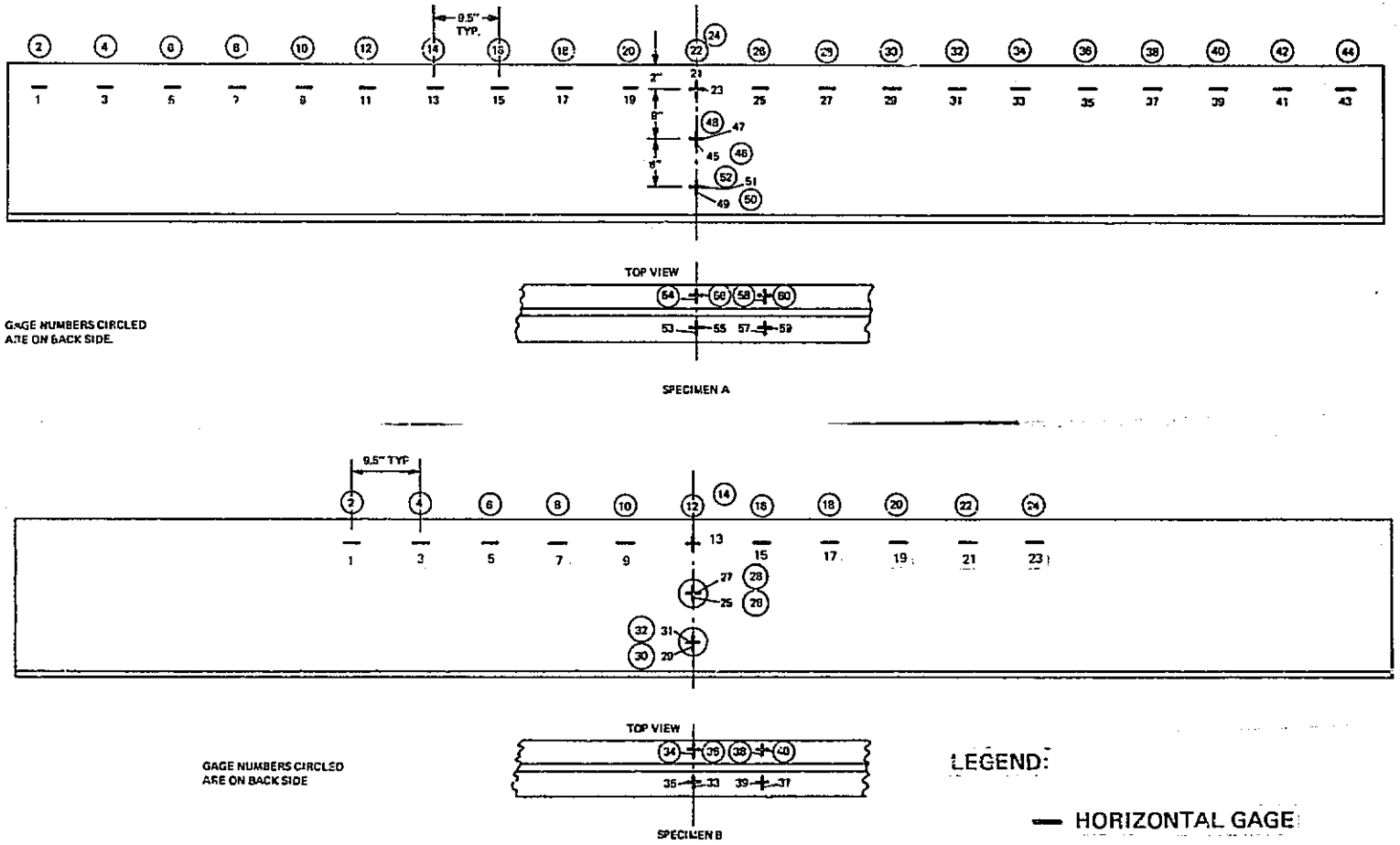

FIGURE AII-1
STRAIN GAGE LOCATIONS, SPECIMENS A AND B

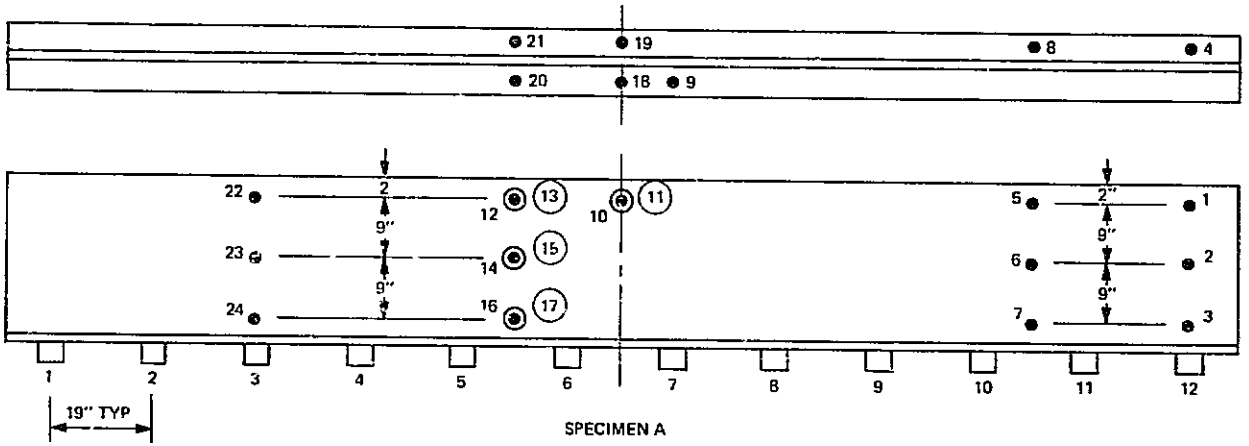

SPECIMEN A

NOTE: CIRCLED DOT INDICATES SENSORS ON BOTH SIDES OF RAIL

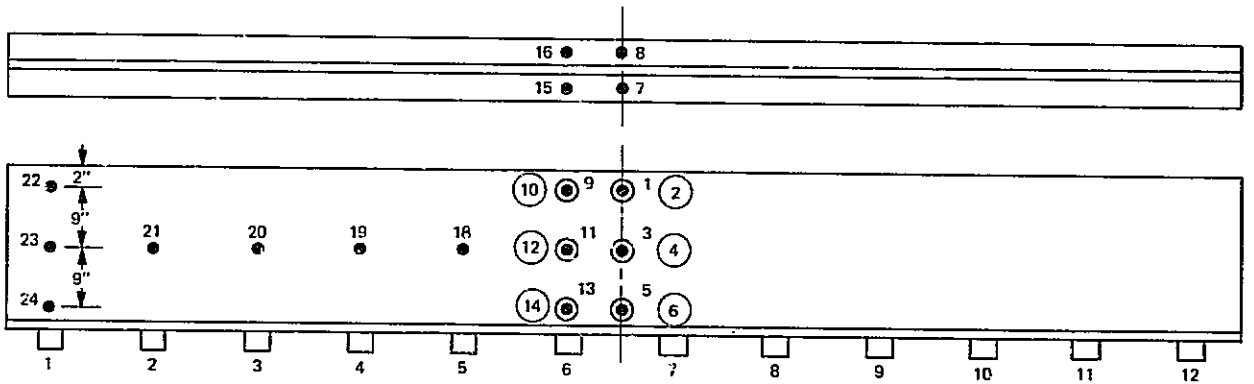

SPECIMEN B

FIGURE AII-2
THERMOCOUPLE LOCATIONS, SPECIMENS A AND B

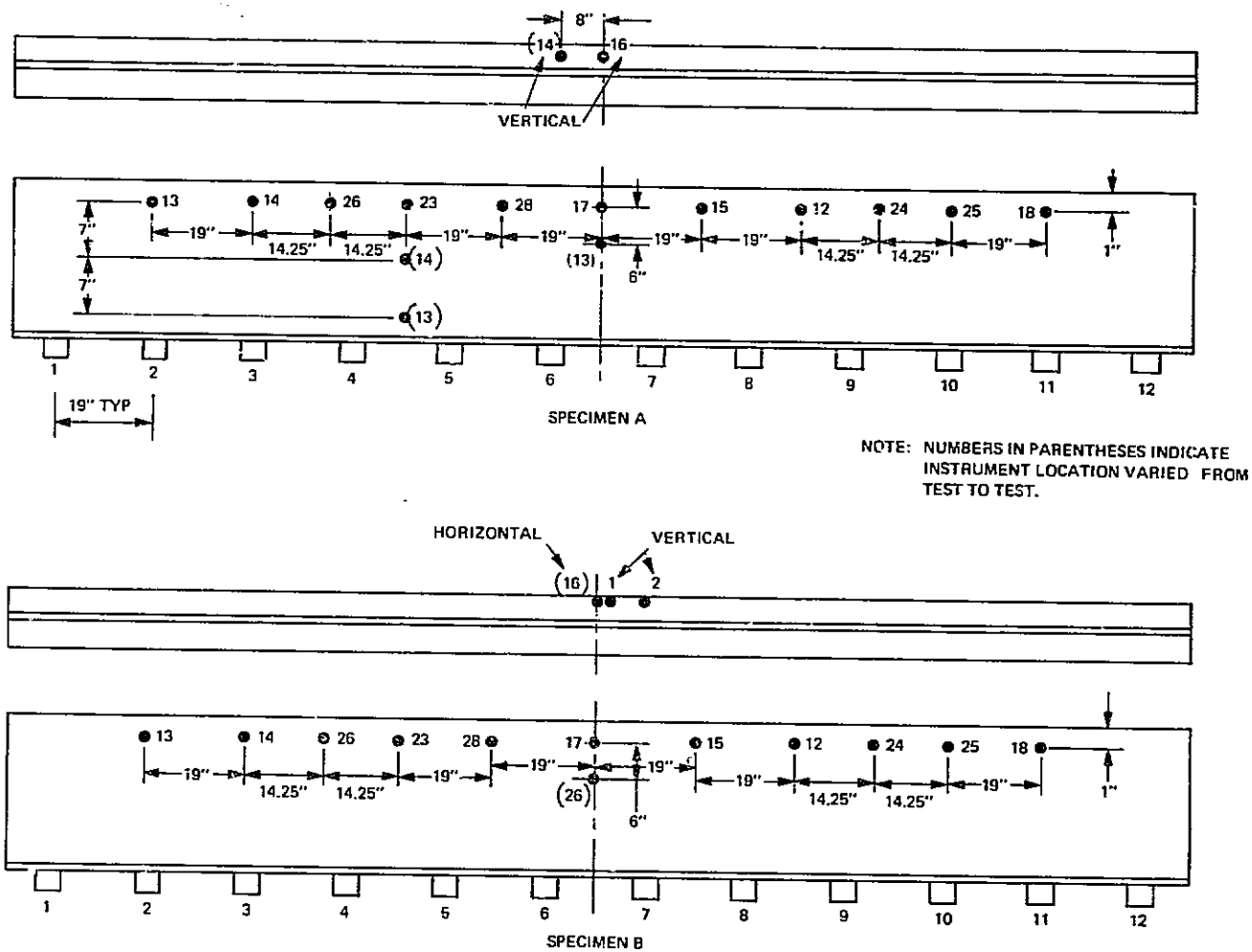

FIGURE AII-3
LVDT LOCATIONS, SPECIMENS A AND B

APPENDIX III
TEST SPECIMEN INSTALLATION PROCEDURE

The procedure for positioning the test specimen in the testing rig, beginning after the subfloor, crossties, and end frame are in position, is as follows:

1. Place the tie plates on the crossties over the predrilled mounting holes.
2. Vertically align the tie plates using shims between the tie plate and crosstie (Figure AIII-1.)
3. Place spring steel clips and coach screws on the tie plates on one side only.
4. Place the rail on the tie plates.
5. Loosely install the spring clip and coach screw on the remaining side.
6. Slide the end billets over the rail ends from above (Figure AIII-2) and center them in the end frames.
7. Shim the rail ends to fit snugly into the slots in the end billets.
8. Survey the end billets to insure vertical alignment. Tighten the lateral leveling pads.
9. Uniformly tighten the longitudinal leveling pads to about 50 ft. lb. to seat the rail in the billets.
10. Loosen the longitudinal leveling pads and retighten them to 4.2 ft. lb. so as not to cause a high initial axial stress.
11. Survey the lateral alignment of the rail base to determine the initial lateral shim pattern and install the lateral shims (Figure AIII-3).
12. Torque the coach screws to 250 ft. lb. and resurvey the lateral alignment of the base flange. Use this data to correct the flange alignment.
13. Survey the lateral alignment of the rail upper edge (Figure AIII-4) and add or remove the vertical shims required to tilt the top edge into alignment.

The alignment survey indicated in step 2 was accomplished using a surveyor's level and height gage readable to 0.001 inch Steps 8-11 used the same gage in conjunction with a transit. Graphs of the final shape of the installed test specimens are presented in Section 3.

The procedure just described is an idealized one and works well only if the predrilled holes in the crossties for the coach screws are precisely located at the desired final location of the tie clips. Two methods can be used to circumvent the possibility of unsatisfactory alignment. First, the holes could be drilled in the crossties after the rail

NASA
L-72-2351

FIGURE AIII-1
VERTICAL POSITIONING OF TIE PLATES

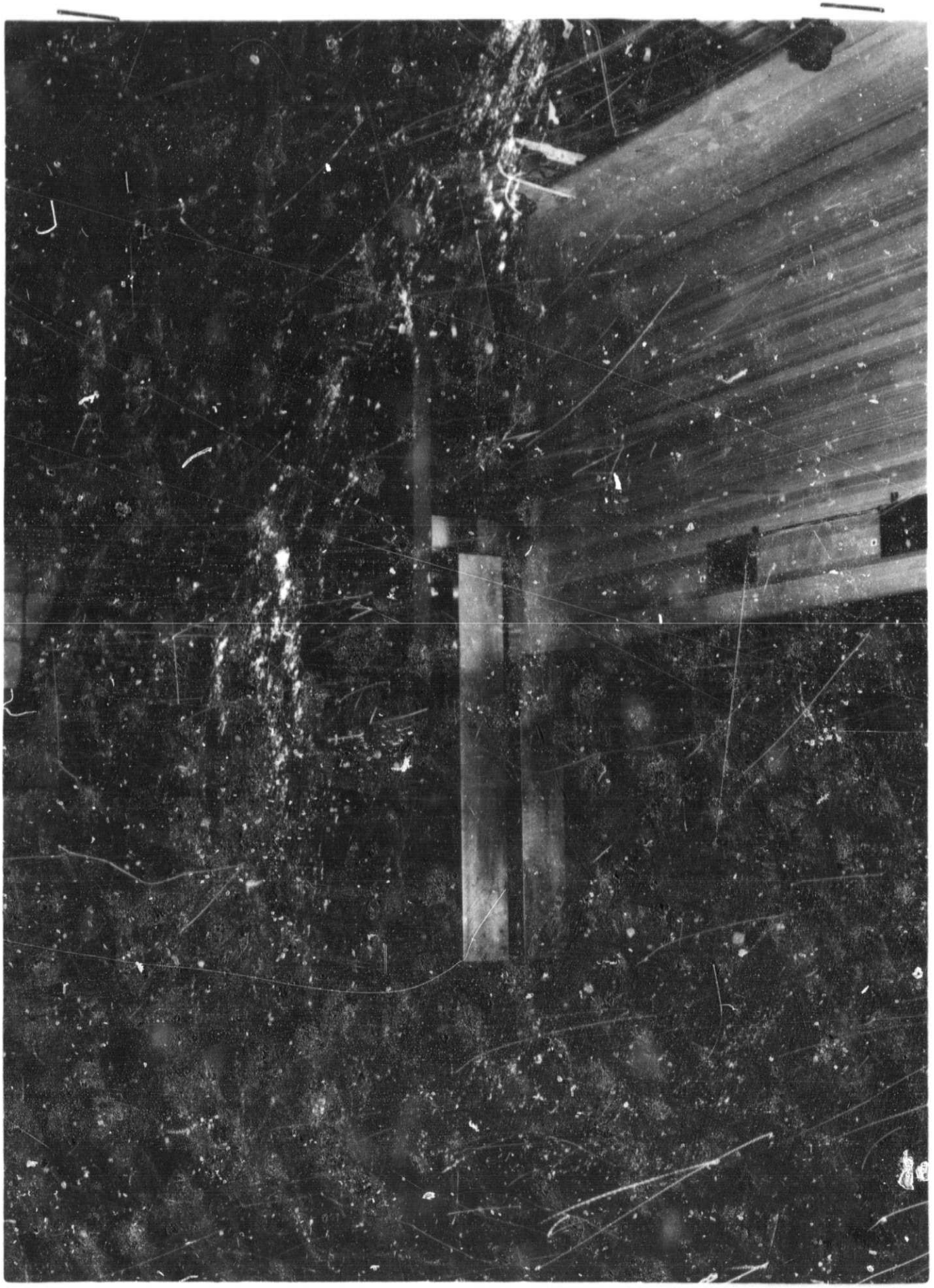

NASA
L-72-2632

FIGURE AIII-2
POSITIONING THE END BILLET

NASA
L-72-2765

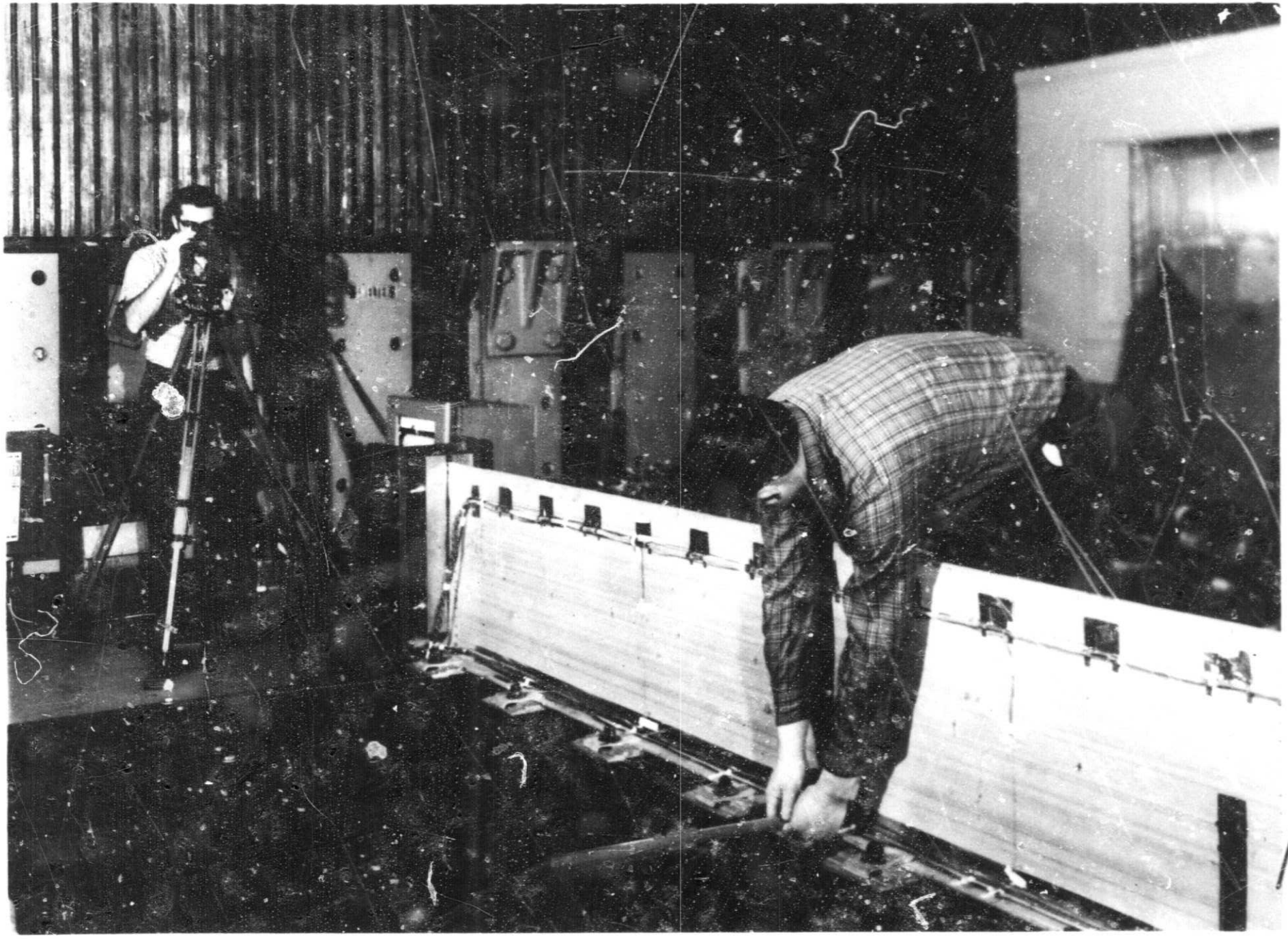

FIGURE AIII-3
LATERAL ALIGNMENT OF BASE FLANGE

NASA
L-72-2766

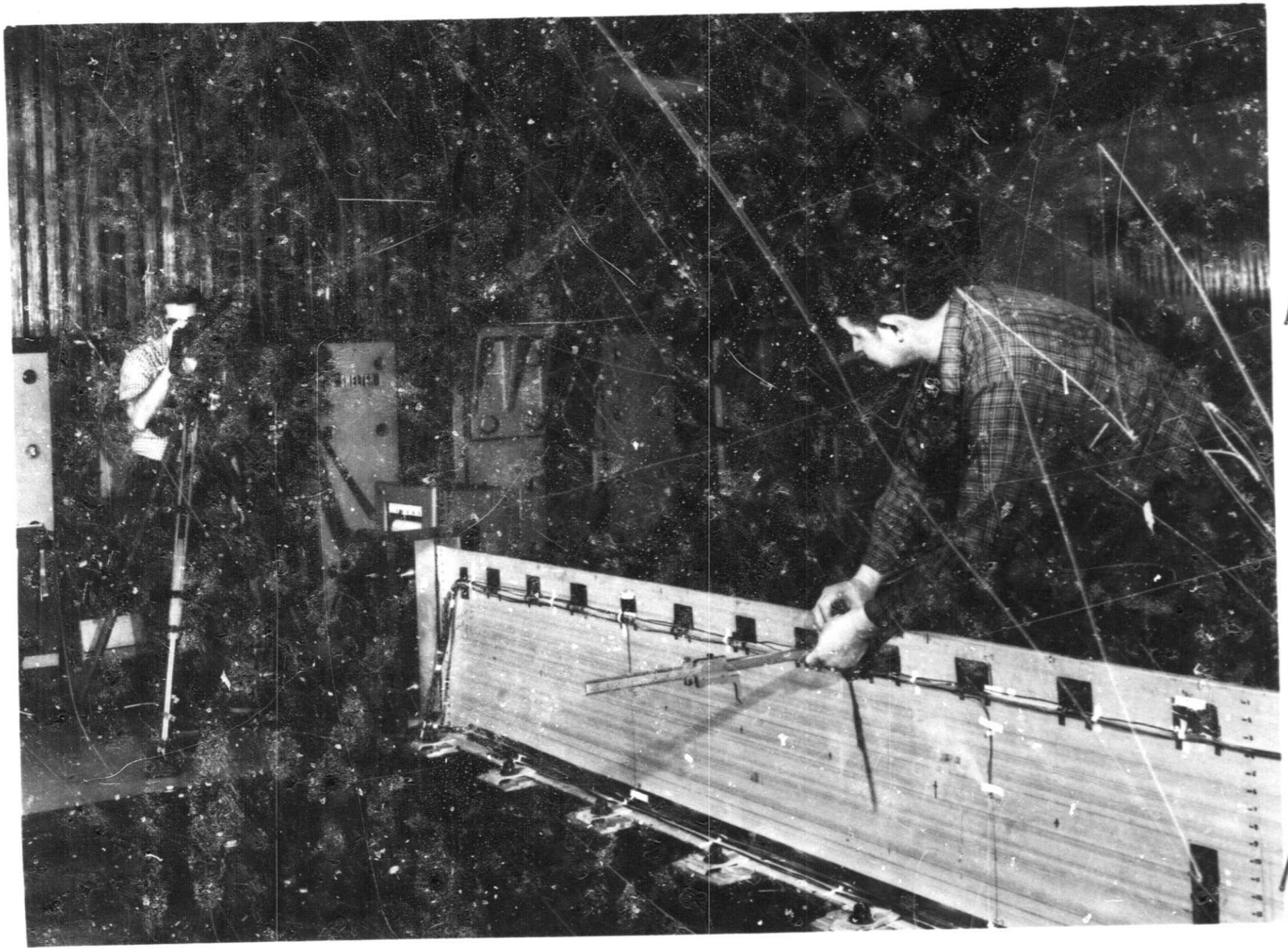

FIGURE AIII-4
LATERAL ALIGNMENT OF RAIL UPPER EDGE

specimen is placed on the tie plates and fixed in the end billets. Second, the pre-drilled holes could be used as described, but the fastening of the crossties to the longitudinal stringers could be performed as the last item (after fastening the tie plates to the ties and fixing the rail in the end billets).